Journal of Medicinal Chemistry

Article

Cite This: J. Med. Chem. XXXX, XXX, XXX−XXX

pubs.acs.org/jmc

Design, Synthesis, and Biological Evaluation of 6-Substituted Thieno[3,2-*d*]pyrimidine Analogues as Dual Epidermal Growth Factor Receptor Kinase and Microtubule Inhibitors

Romeo Romagnoli,*[,†] Filippo Prencipe,[†] Paola Oliva,[†] Stefania Baraldi,[†] Pier Giovanni Baraldi,[†] Santiago Schiaffino Ortega,[‡] Mariem Chayah,[‡] Maria Kimatrai Salvador,[‡] Luisa Carlota Lopez-Cara,*[,‡] Andrea Brancale,[§] Salvatore Ferla,[§] Ernest Hamel,[∥] Roberto Ronca,[⊥] Roberta Bortolozzi,[#] Elena Mariotto,[#] Elena Mattiuzzo,[#] and Giampietro Viola*[,#,▽]

[†]Dipartimento di Scienze Chimiche e Farmaceutiche, Università degli Studi di Ferrara, Via Luigi Borsari 46, 44121 Ferrara, Italy

[‡]Departamento de Química Farmacéutica y Orgánica, Facultad de Farmacia, Campus de Cartuja s/n, 18071 Granada, Spain

[§]School of Pharmacy and Pharmaceutical Sciences, Cardiff University, King Edward VII Avenue, Cardiff CF10 3NB, U.K.

[∥]Screening Technologies Branch, Developmental Therapeutics Program, Division of Cancer Treatment and Diagnosis, Frederick National Laboratory for Cancer Research, National Cancer Institute, National Institutes of Health, Frederick, Maryland 21702, United States

[⊥]Dipartimento di Medicina Molecolare e Traslazionale Unità di Oncologia Sperimentale ed Immunologia, Università di Brescia, 25123 Brescia, Italy

[#]Dipartimento di Salute della Donna e del Bambino, Laboratorio di Oncoematologia, Università di Padova, 35131 Padova, Italy

[▽]Istituto di Ricerca Pediatrica (IRP), Corso Stati Uniti 4, 35128 Padova, Italy

Supporting Information

ABSTRACT: The clinical evidence for the success of tyrosine kinase inhibitors in combination with microtubule-targeting agents prompted us to design and develop single agents that possess both epidermal growth factor receptor (EGFR) kinase and tubulin polymerization inhibitory properties. A series of 6-aryl/heteroaryl-4-(3′,4′,5′-trimethoxyanilino)thieno[3,2-*d*]-pyrimidine derivatives were discovered as novel dual tubulin polymerization and EGFR kinase inhibitors. The 4-(3′,4′,5′-trimethoxyanilino)-6-(*p*-tolyl)thieno[3,2-*d*]pyrimidine derivative **6g** was the most potent compound of the series as an antiproliferative agent, with half-maximal inhibitory concentration (IC_{50}) values in the single- or double-digit nanomolar range. Compound **6g** bound to tubulin in the colchicine site and inhibited tubulin assembly with an IC_{50} value of 0.71 μM, and **6g** inhibited EGFR activity with an IC_{50} value of 30 nM. Our data suggested that the excellent in vitro and in vivo profile of **6g** may be derived from its dual inhibition of tubulin polymerization and EGFR kinase.

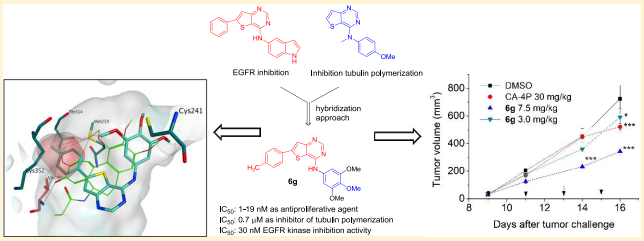

INTRODUCTION

Cellular microtubules are formed by the noncovalent polymerization of α- and β-tubulin heterodimers and act as an essential element of the cytoskeleton. Microtubules are crucial for multiple functions in cells, especially the development and function of the mitotic spindle during mitosis, but also for establishing the shape of the cell, intracellular transport, secretion, and cell movement.[1] Their importance for cell structure and function, together with their long history of utility in cancer chemotherapy, has made microtubules important for anticancer drug discovery, and agents that target them are among the most reliable chemotherapeutics.[2] A substantial number of compounds, representing many chemotypes, bind to tubulin or microtubules and inhibit or enhance tubulin polymerization.[3] Moreover, several small molecules inhibiting tubulin polymerization are able to damage the already existing vasculature in developing tumors, acting as vascular-disrupting agents (VDAs).[4]

Originally derived from a South African tree,[5] combretastatin A-4 (CA-4, **1a**, Figure 1) is a widely studied molecule that inhibits tubulin assembly by binding to the colchicine site.[6] The disodium phosphate prodrug of CA-4 (CA-4P, **1b**) is water-soluble, and there have been promising results with **1b** as a tumor VDA in phase II clinical trials.[7] The properties of CA-4, including its simple structure and its potent destructive effects on tumor blood vessels, have made **1a** widely studied by medicinal chemists.[8]

Received: September 6, 2018
Published: January 11, 2019

DOI: 10.1021/acs.jmedchem.8b01391
J. Med. Chem. XXXX, XXX, XXX−XXX

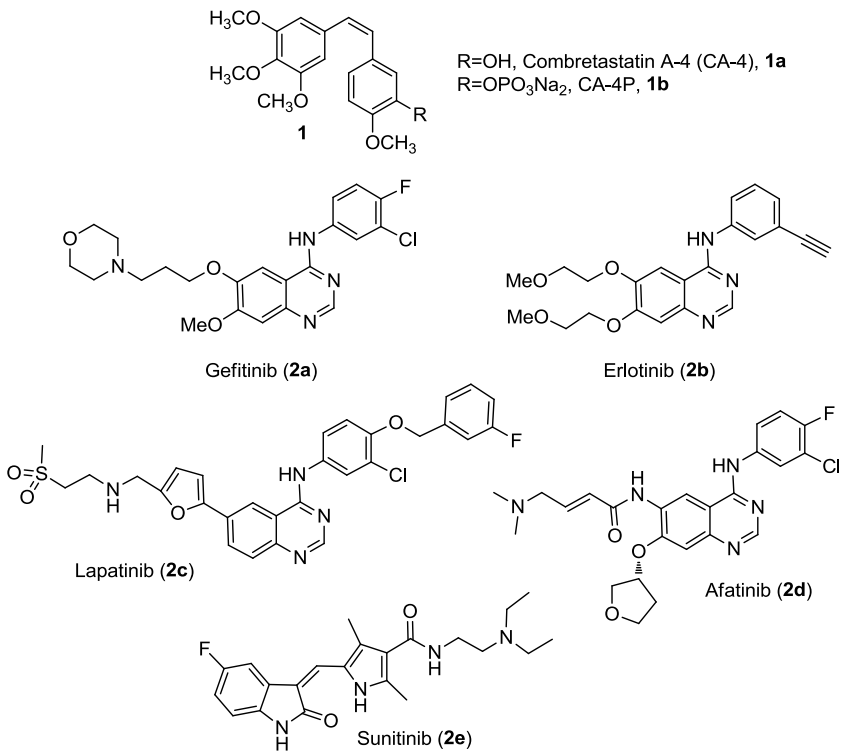

Figure 1. Structures of tubulin-depolymerizing agents CA-4 and CA-4P and selected epidermal growth factor receptor (EGFR) (**2a**−**d**) and vascular endothelial growth factor receptor-2 (VEGFR-2) (**2e**) tyrosine kinase inhibitors.

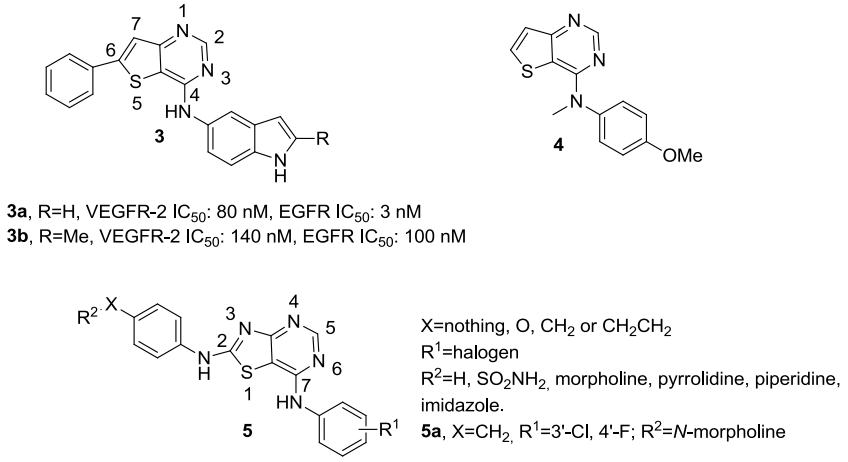

Figure 2. Chemical structures of representative thieno[3,2-*d*]pyrimidines and thiazolo[4,5-*d*]pyrimidines as known tubulin polymerization (**4**) and EGFR kinase (**3** and **5**) inhibitors.

A growing body of evidence has shown that antimitotic agents, and in particular microtubule-destabilizing drugs, have multiple effects beyond mitosis.[9] Several lines of evidence suggested mixed mechanisms that are not so far fully understood to explain the activities of tubulin-binding agents, and these mechanisms probably extend beyond simple antimitotic effects. Moreover, there is evidence that the efficacy of microtubule-targeting agents also involves interphase effects.[10]

Signal transduction in mammalian cells involves many receptor kinases. Particularly important is the epidermal growth factor receptor, which is a transmembrane-bound molecule that has important regulatory functions affecting tumor growth and progression. These include cell proliferation, differentiation, migration, apoptosis, and angiogenesis.[11] EGFR kinase, consisting of ErB1 and HER1, belongs to the ErbB family of kinases, which also includes human epidermal growth factor receptor-2 (subunits: HER2 and ErbB-2), human epidermal growth factor receptor-3 (subunits: HER3 and ErbB-3), and human epidermal growth factor receptor-4 (subunits: HER4 and ErbB-4).[12] Among the known receptor tyrosine kinases (RTKs), those of the ErbB family, in particular, EGFR and HER2, have been extensively studied and clinically validated as targets for cancer therapies, being over-expressed in a wide number of human tumors and associated with cancer proliferation, angiogenesis, and metastasis.[13] With no bound ligand, EGFR is in monomeric form of the cell surface. When ligand is bound, EGFR forms homodimers with itself and heterodimers with other ErbB family members.[14] There are currently eight drugs approved by

DOI: 10.1021/acs.jmedchem.8b01391
J. Med. Chem. XXXX, XXX, XXX−XXX

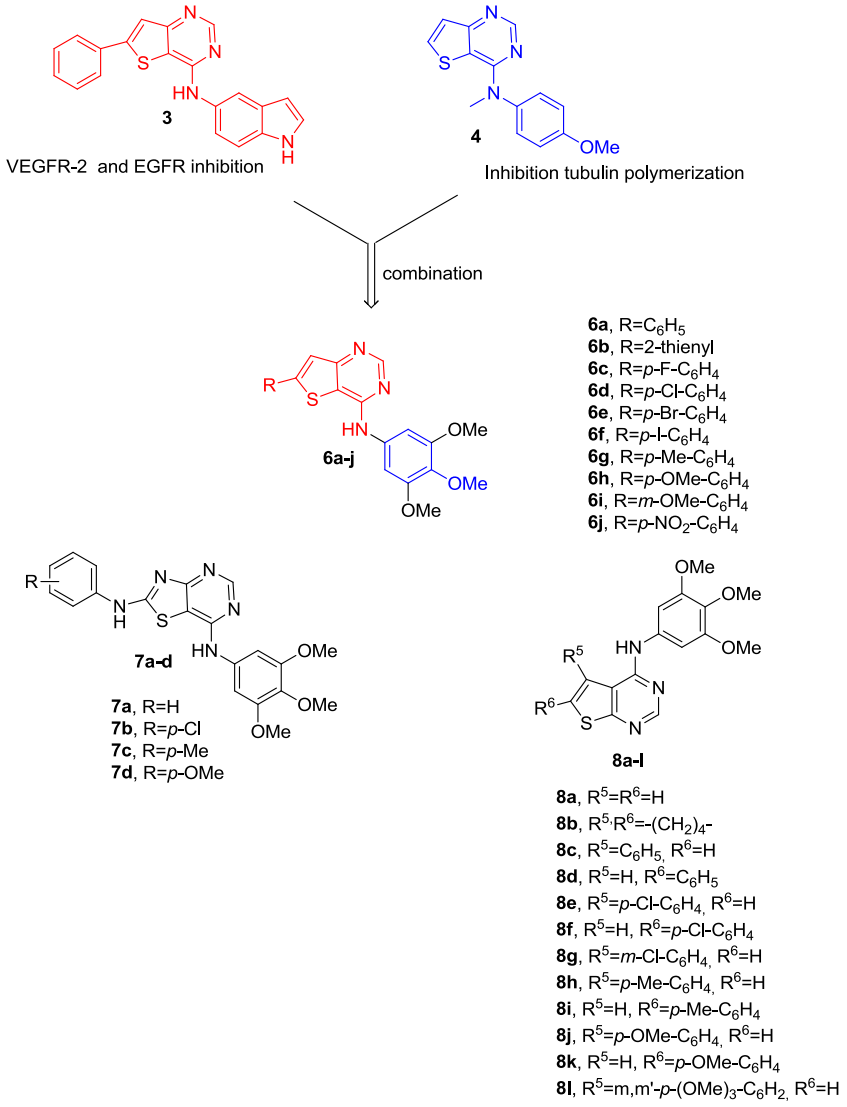

Figure 3. Design strategy for thieno[3,2-*d*]pyrimidines **6a–j**. Target compounds containing the thiazolo[4,5-*d*]pyrimidine (**7a–d**) and thieno[2,3-*d*]pyrimidine (**8a–l**) scaffolds.

the Food and Drug Administration (FDA) targeting this family: four monoclonal antibodies (trastuzumab, cetuximab, panitumumab, and pertuzumab) and four small-molecule inhibitors based on a central 4-aminoarylquinazoline core [gefitinib (**2a**), erlotinib (**2b**), lapatinib (**2c**), and afatinib (**2d**)].[15] These latter synthetic EGFR inhibitors have been approved by the FDA for the treatment of patients with non-small-cell lung cancer (NSCLC).[16,17] Unfortunately, the duration of benefit derived from the therapy based on tyrosine kinase inhibitors is relatively short because of the development of acquired resistance.[17a] The development of multitargeted inhibitors represents a valid approach to overcome the acquired drug resistance to tyrosine kinase inhibitors.[17b] Twelve clinical trials were found on the clinicaltrials.gov site (accessed in October 2018) in which the FDA-approved EGFR kinase inhibitors gefitinib, erlotinib, and lapatinib were being used in combination with the microtubule-targeting agents docetaxel, vinorelbine, paclitaxel, and other chemotherapeutic agents for the treatment of a variety of cancers including lung cancer, head and neck cancer, and hepatocellular carcinoma.[18]

A large number of thienopyrimidine derivatives have been reported to show remarkable antitumor activity against different cancer types by means of inhibiting multiple enzymes, as well as by modulating the activity of many receptors.[19] In an effort to develop nonquinazoline EGFR inhibitors, using the strategy known as "scaffold hopping", bioisosteric thieno[2,3-*d*]pyrimidine and thieno[3,2-*d*]pyrimidine scaffolds have been reported as interesting structural elements employed for the development of novel EGFR or EGFR with vascular endothelial growth factor receptor-2 (VEGFR-2) dual inhibition.[20]

Munchhof et al. reported the design and structure–activity relationship (SAR) of a series of 6-aryl-substituted thieno[3,2-*d*]pyrimidines with general structure **3**, identified as VEGFR-2 and EGFR dual inhibitors (Figure 2).[21] Kemnitzer and his colleagues reported the discovery of *N*-methyl-4-(methoxyanilino)thieno[3,2-*d*]pyrimidine **4** as a potent apoptosis inducer through inhibition of tubulin assembly, with half-maximal inhibitory concentration (IC_{50}) <1 μM in the tubulin polymerization assay.[22] This compound inhibited the growth of a panel of five cancer cell lines (T-47D, HT-29, H-1299, MX-1, and MDAAMB 435) with IC_{50} values ranging

DOI: 10.1021/acs.jmedchem.8b01391
J. Med. Chem. XXXX, XXX, XXX–XXX

Scheme 1. Synthesis of Thieno[3,2-*d*]pyrimidines 6a−j and Thiazolo[4,5-*d*]pyrimidines 7a−d[a]

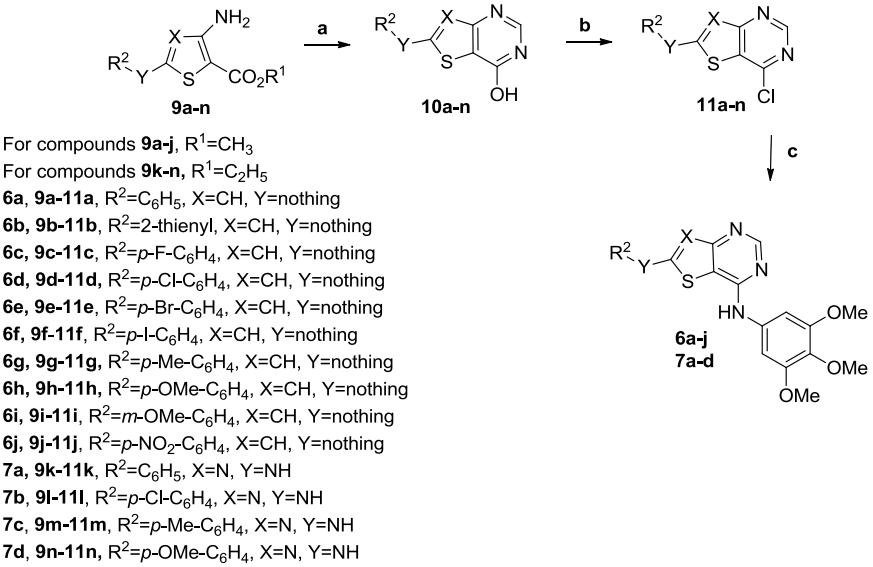

For compounds **9a-j**, R^1=CH_3
For compounds **9k-n,** R^1=C_2H_5
6a, **9a-11a**, R^2=C_6H_5, X=CH, Y=nothing
6b, 9b-11b, R^2=2-thienyl, X=CH, Y=nothing
6c, 9c-11c, R^2=*p*-F-C_6H_4, X=CH, Y=nothing
6d, 9d-11d, R^2=*p*-Cl-C_6H_4, X=CH, Y=nothing
6e, 9e-11e, R^2=*p*-Br-C_6H_4, X=CH, Y=nothing
6f, 9f-11f, R^2=*p*-I-C_6H_4, X=CH, Y=nothing
6g, 9g-11g, R^2=*p*-Me-C_6H_4, X=CH, Y=nothing
6h, 9h-11h, R^2=*p*-OMe-C_6H_4, X=CH, Y=nothing
6i, 9i-11i, R^2=*m*-OMe-C_6H_4, X=CH, Y=nothing
6j, 9j-11j, R^2=*p*-NO_2-C_6H_4, X=CH, Y=nothing
7a, 9k-11k, R^2=C_6H_5, X=N, Y=NH
7b, **9l-11l**, R^2=*p*-Cl-C_6H_4, X=N, Y=NH
7c, **9m-11m**, R^2=*p*-Me-C_6H_4, X=N, Y=NH
7d, **9n-11n,** R^2=*p*-OMe-C_6H_4, X=N, Y=NH

[a]Reagents and conditions. (a) $HCONH_2$, 180 °C; (b) $POCl_3$, 110 °C; (c) 3,4,5-trimethoxyaniline, isopropanol, reflux.

from 4 to 40 nM. Much research has been conducted on the structural modification of the thieno[3,2-*d*]pyrimidine skeleton, with the 4-, 6-, and 7-positions as the main targets for chemical modifications to increase antitumor activity.[23]

Lin et al. have also reported a series of 2,7-diaminothiazolo-[4,5-*d*]pyrimidines with general formula **5**, with various structural modifications at the 2- and 7-positions, as potent EGFR inhibitors, with IC_{50} values ranging from micromolar to single-digit nanomolar.[24] Compound **5a**, characterized by potent and selective EGFR activity (IC_{50}: 12 nM), proved to be active in vitro as an antiproliferative agent against the human ovarian adenocarcinoma (SK-OV-3) cell line, with an IC_{50} value of 0.57 μM. Unfortunately, compound **5a** showed no in vivo antitumor efficacy in a tumor xenograft model in nude mice.

Our findings caused us to use the thieno[3,2-*d*]pyrimidine scaffold for optimization of the pharmacophore, which was maintained for the discovery of new antitumor agents. We replaced the 5′-aminoindole side chain at the C-4 position of 6-phenylthieno[2,3-*d*]pyrimidine derivatives with general structure **3** with a 3′,4′,5′-trimethoxyanilino moiety to furnish a first series of 4-(3′,4′,5′-trimethoxyanilino)-6-aryl/heteroaryl-thieno[3,2-*d*]pyrimidine derivatives with general structure **6** (Figure 3). By maintaining the 3′,4′,5′-trimethoxyanilino group at the 4-position, the first stage of our study was to evaluate the steric and electronic effects of different substituents on the benzene portion at the C-6 position of the 4-(3′,4′,5′-trimethoxyanilino)thieno[2,3-*d*]pyrimidine nucleus. Besides hydrogen, the examined substituents included electron-withdrawing groups (EWGs), such as F, Cl, Br, I, and NO_2, and the electron-releasing methyl and methoxy groups (electron-releasing groups (ERGs)). The bioisosteric replacement of phenyl with the thien-2-yl ring was also explored.

All of the newly synthesized agents contained the 3′,4′,5′-trimethoxyanilino moiety at the common C-4 position of the thieno[2,3-*d*]pyrimidine nucleus and isomeric thieno[3,2-*d*]pyrimidine nucleus, as well as at the C-7 position of the thiazolo[4,5-*d*]pyrimidine system. The rationale for this was the well-documented requirement for a trimethoxyphenyl group in numerous colchicine site inhibitors.[25]

In the second small series of compounds, the thiophene nucleus was replaced by the bioisosteric thiazole ring to obtain the derivatives **7a−d**, characterized by the presence of an anilino moiety at its C-7 position. The electron-withdrawing chlorine atom (**7b**) and the electron-releasing methyl and methoxy groups (**7c** and **7d**, respectively) were introduced at the para-position of the phenyl portion of the anilino moiety.

In a third series of compounds, **8a−l**, we explored the replacement of the thieno[3,2-*d*]pyrimidine system, which characterizes derivatives with general structure **6**, by the isomeric thieno[2,3-*d*]pyrimidine nucleus. The SAR was investigated by the insertion of different substituents (Cl, Me, or OMe) on the phenyl ring at the C-5 or C-6 position of the 4-(3′,4′,5′-trimethoxyanilino)thieno[2,3-*d*]pyrimidine core.

These three series of compounds, obtained by replacing the thieno[3,2-*d*]pyrimidine scaffold with the isomeric thieno[2,3-*d*]pyrimidine and the bioisosteric thiazolo[4,5-*d*]pyrimidine skeletons, were designed to determine the potential of incorporating in a single molecule both VEGFR-2 and/or EGFR kinase inhibition and antitubulin activity.

The bioisosteric replacement of the thiophene ring of the structure motif of the thieno[2,3-*d*]pyrimidine nucleus with a furan or pyrrole provided two series of furo[2,3-*d*]pyrimidine and pyrrolo[3,2-*d*]pyrimidine derivatives, respectively, identified by Gangjee et al. as multitarget receptor tyrosine kinase and microtubule inhibitors.[26−28] A literature search also revealed that recent studies have yielded different series of chemically diverse small molecules acting as EGFR kinase and tubulin polymerization inhibitors derived from anthranilic acid[29] or benzo[*b*]furan[30] or obtained by replacing the quinazoline core of compounds **2a−d** with a quinazolinone[31,32] or triazolo[4,3-*a*]quinoxaline[33] scaffold.

RESULTS AND DISCUSSION

Chemistry. Preparation of thieno[3,2-*d*] pyrimidine and thiazolo[4,5-*d*]pyrimidine derivatives **6a−j** and **7a−d**, respec-

DOI: 10.1021/acs.jmedchem.8b01391
J. Med. Chem. XXXX, XXX, XXX−XXX

Scheme 2. Synthesis of Thieno[2,3-*d*]pyrimidines (8a–l)[a]

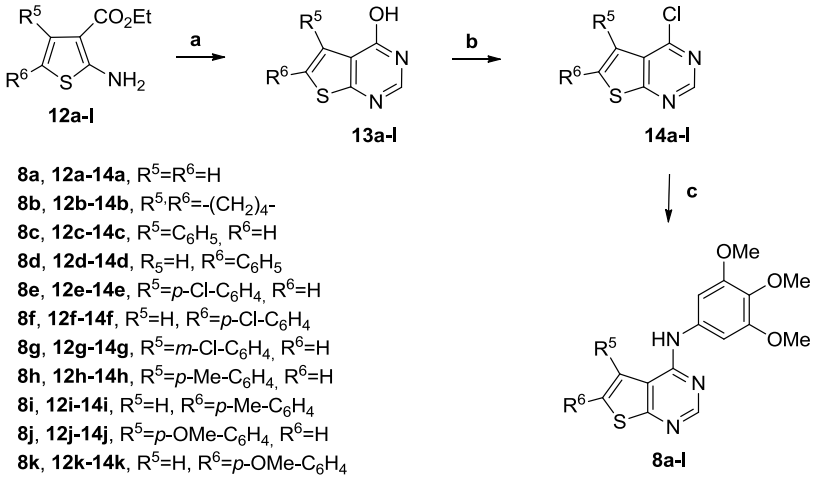

[a]Reagents and conditions. (a) $HCONH_2$, 180 °C; (b) $POCl_3$, 110 °C; (c) 3,4,5-trimethoxyaniline, isopropanol, reflux.

Table 1. In Vitro Cell Growth Inhibitory Effects of Compounds 6a–j and CA-

	IC_{50}[a] (μM)				
compound	A549	HeLa	HT-29	Jurkat	RS4;11
6a	2.3 ± 0.7	0.17 ± 0.02	0.35 ± 0.06	0.01 ± 0.006	0.26 ± 0.10
6b	5.1 ± 1.9	1.7 ± 0.8	0.21 ± 0.07	0.08 ± 0.03	0.36 ± 0.1
6c	13.5 ± 3.0	0.45 ± 0.09	1.9 ± 0.8	0.26 ± 0.04	1.9 ± 0.3
6d	0.60 ± 0.11	0.09 ± 0.03	0.087 ± 0.033	0.003 ± 0.001	0.005 ± 0.002
6e	0.53 ± 0.16	0.22 ± 0.09	0.15 ± 0.04	0.03 ± 0.005	0.19 ± 0.04
6f	0.77 ± 0.26	0.28 ± 0.15	0.25 ± 0.13	0.30 ± 0.06	0.17 ± 0.04
6g	0.019 ± 0.008	0.001 ± 0.0005	0.02 ± 0.007	0.001 ± 0.0005	0.002 ± 0.001
6h	0.43 ± 0.13	0.17 ± 0.08	0.06 ± 0.04	0.005 ± 0.001	0.004 ± 0.001
6i	8.8 ± 1.9	3.2 ± 0.1	3.3 ± 0.8	3.0 ± 1.0	5.4 ± 1.3
6j	1.1 ± 0.3	4.9 ± 1.4	6.3 ± 1.4	2.0 ± 0.3	1.3 ± 0.4
CA-4	0.18 ± 0.05	0.004 ± 0.0001	3.1 ± 0.1	0.005 ± 0.0001	0.001 ± 0.0001

[a]IC_{50} = compound concentration required to inhibit tumor cell proliferation by 50%. Data are expressed as the mean ± standard error (SE) from the dose–response curves of at least three independent experiments.

tively, was accomplished using the general convergent synthetic route shown in Scheme 1. Cyclization of methyl 5-aryl/heteroayl-3-aminothiophene-2-carboxylate and ethyl 2-anilino-4-aminothiazole-5-carboxylate **9a–j** and **9k–n**, respectively, with formamide ($HCONH_2$) yielded the corresponding 6-aryl/heteroaryl-thieno[3,2-*d*]pyrimidin-4(3*H*)-ones **10a–j** and 2-arylaminothiazolo[4,5-*d*]pyrimidin-7(6*H*)-ones **10k–n**. The subsequent chlorination of the carbonyl group with phosphorus oxychloride ($POCl_3$) provided 4-chlorothieno[3,2-*d*]pyrimidine and 7-chlorothiazolo[4,5-*d*]pyrimidine derivatives **11a–j** and **11k–n**, respectively. Finally, the nucleophilic substitution with 3,4,5-trimethoxyaniline in refluxing isopropanol furnished the final compounds **6a–j** and **7a–d**, respectively.

The isomeric 4-(3′,4′,5′-trimethoxyanilino)-thieno[2,3-*d*]-pyrimidine derivatives **8a–l** were synthesized following the procedure reported in Scheme 2. Thieno[2,3-*d*]pyrimidin-4(3*H*)-one derivatives **13a–l** variously substituted at their C-5 or C-6 position were prepared by cyclocondensation of ethyl 2-aminothiophene-3-carboxylate derivatives **12a–l** with $HCONH_2$ at 180 °C for 8–12 h. These intermediates were subjected to chlorination by the action of $POCl_3$ at reflux to furnish the 4-chlorothieno[2,3-*d*]pyrimidine analogues **14a–l**. The final step of the synthesis involved nucleophilic displacement of the 4-chloride atom of **14a–l** with 3,4,5-trimethoxyaniline in refluxing isopropanol to obtain the 4-(3′,4′,5′-trimethoxyanilino)thieno[3,2-*d*]pyrimidine derivatives **8a–l**.

In Vitro Antiproliferative Activities. Table 1 summarizes the antiproliferative effects of 4-(3′,4′,5′-trimethoxyanilino)-6-substituted thieno[3,2-*d*]pyrimidine derivatives **6a–j** against a panel of five human cancer cell lines [including EGFR wild-type ($EGFR^{wt}$) NSCLC A549 cells], using CA-4 as the reference compound. The corresponding thieno[2,3-*d*]-pyrimidine isomers **7a–d** and the 2-anilino-7-(3′,4′,5′-trimethoxyanilino)thiazolo[4,5-*d*]pyrimidines **8a–l** were also evaluated for their activities on the same panel of cells, but because they were all inactive (IC_{50} > 10 μM), with only a few exceptions on selected cancer cell lines (derivatives **6h**, **6k**, and **6l**), these biological data are presented in Tables 1S and 2S (Supporting Information), respectively.

The unsubstituted phenyl derivative **6a** was weakly active (IC_{50}: 2.3 μM) against A549, moderately potent against HeLa, HT-29, and RS4;11 with IC_{50} values of 0.17, 0.35, and 0.26 μM, respectively, but showed high activity (IC_{50}: 10 nM) against Jurkat cells. The bioisosteric 2-thienyl analogue **6b** was 2-, 8-, and 10-fold less active than **6a** against A549, Jurkat, and

DOI: 10.1021/acs.jmedchem.8b01391
J. Med. Chem. XXXX, XXX, XXX–XXX

HeLa cells, respectively, whereas the difference in potency between **6a** and **6b** was minimal in RS4;11 cells. **6a** was less active than **6b** only in HT-29 cells, with IC_{50} values of 0.35 and 0.21 μM, respectively.

The introduction of electron-releasing or electron-withdrawing substituents at the para-position of the phenyl ring at the C-6 position of the thieno[3,2-*d*]pyrimidine nucleus appeared to have considerable biological effects, enhancing antiproliferative activity compared to that of the unsubstituted phenyl analogue **6a**. These compounds include the *p*-Cl (**6d**; IC_{50}: 3−600 nM), *p*-Me (**6g**; IC_{50}: 1−20 nM), and *p*-OMe (**6h**; IC_{50}: 4−430 nM) derivatives. The *p*-tolyl derivative **6g** displayed the strongest growth inhibitory activity against A549, HeLa, HT-29, Jurkat, and RS4;11, with IC_{50} values of 19, 1, 20, 1, and 2 nM, respectively.

A *para*-fluoro group in the phenyl ring (compound **6c**) caused a reduction of activity by 2−26-fold relative to that of the unsubstituted phenyl derivative **6a**, whereas the presence of other halogen groups led to an improvement in antiproliferative activity. As the bulk of the halide group increased from a fluoro to a chloro moiety, the resulting compound **6d** produced a 5- to 87-fold increase in antiproliferative activity in the five cell lines. Replacing chlorine with bromine (**6e**) reduced the activity by 2−38-fold against four of the five cancer cell lines, but **6d** and **6e** were equally potent against A549 cells. For the *p*-Br and *p*-I derivatives **6e** and **6f**, respectively, nearly identical activities were observed in three of the five cancer cell lines, the exception being the HT-29 and Jurkat cells, in which **6f** was 2- and 10-fold more potent than **6e**, respectively.

The small and weak electron-releasing methyl group at the para-position of the phenyl ring, to yield derivative **6g**, improved the antiproliferative activity significantly relative to that of **6a**. Derivative **6g** exhibited the greatest cell growth inhibitory effects among the tested compounds, with IC_{50} values of 1−20 nM against all cell lines, as compared with the range 0.8−3100 nM obtained with CA-4. Compound **6g** was equipotent with CA-4 against RS4;11 cells, whereas it was from 2- to 1.5×10^5 times more active against the other four cancer cell lines.

A *para*-methoxy group in the phenyl ring (**6h**), a more potent electron-releasing group than the methyl of **6h**, caused a marked reduction (2−170-fold) in activity against the tumor cell lines. Thus, the two substituents, despite their structural similarity, are not biologically equivalent. The reduction in activity was more evident, 23- and 170-fold, against A549 and HeLa, respectively, whereas only a 2-, 3-, and 5-fold reduced activity was observed against RS4;11, HT-29, and Jurkat cells, respectively.

Compound **6i**, with a methoxy group at the meta-position of the phenyl ring, was 1−4 orders of magnitude less active than the *para*-methoxy isomer **6h**, indicating that the position of the methoxy group was important for in vitro activity.

Among the strong electron-withdrawing groups, the small polar nitro substituent, intermediate in size between those of chlorine and bromine, when placed in the para-position of the phenyl ring, furnished a compound (**6j**) with reduced antiproliferative activity (IC_{50}: 1.1−6.3 μM) relative to that of the unsubstituted phenyl derivative **6a**.

Inhibition of Tubulin Polymerization and Colchicine Binding. We anticipated that at least some of the compounds would have antitubulin activity, and **6a−b** and **6d−h** were examined for inhibitory effects on tubulin assembly and on the binding of colchicine to tubulin in comparison with CA-4 (Table 2).

Table 2. Inhibition of Tubulin Polymerization and Colchicine Binding by Compounds 6a−b, 6d−h, and CA-4 (1a)

compound	tubulin assembly,[a] IC_{50} ± SD (μM)	colchicine binding,[b] % inhibition ± SD
6a	10 ± 2	n.d.[c]
6b	18 ± 1	n.d.
6d	3.3 ± 0.3	36 ± 3
6e	2.5 ± 0.3	35 ± 4
6f	2.5 ± 0.2	35 ± 2
6g	0.71 ± 0.05	76 ± 0.7
6h	2.8 ± 0.2	31 ± 3
CA-4	1.2 ± 0.1	98 ± 0.7

[a]Inhibitory effects on the assembly of 10 μM purified tubulin. [b]In the experiments to evaluate compound effects on the binding of [^{3}H]colchicine to purified tubulin, the protein was 1.0 μM and the radiolabeled colchicine and inhibitory compound were both at 5.0 μM. [c]n.d.: not done.

Compounds **6e−h** strongly inhibited tubulin assembly, with derivative **6g** as the most active of the series, being almost 2-fold more active than CA-4 in this assay (IC_{50}: 0.71 and 1.2 μM for **6g** and CA-4, respectively). Compounds **6e**, **6f**, and **6h** were half as active (IC_{50}: 2.5, 2.5, and 2.8 μM, respectively) and **6d** about one-third as active (IC_{50}: 3.3 μM) as CA-4. Compounds **6a** and **6b** showed weak antitubulin polymerization activities (IC_{50}: 10 and 18 μM, respectively), which were consistent with their low antiproliferative activity. Thus, in the two tubulin biochemical assays, compound activities were similar, with **6g** the most active (even more active than CA-4 in the polymerization assay) and **6a** and **6b** the least active in the polymerization assay. These data are consistent with the conclusion that tubulin was an intracellular target of the tested compounds.

EGFR and VEGFR-2 Kinase Inhibitory Activity Assay. Compounds **6a−b** and **6d−h** were further evaluated for their EGFR and VEGFR-2 kinase inhibitory activities. The approved VEGFR-2 and EGFR inhibitory agents sunitinib and erlotinib (**2b**), respectively, were used as positive controls. The data compiled in Table 3 showed potent inhibition of $EGFR^{wt}$ kinase by compounds **6a−b** and **6f−h**, but no inhibition of VEGFR-2 (IC_{50} > 1 μM) was observed. All tested molecules, with the exception of **6d** and **6e**, were more potent than

Table 3. EGFR Inhibitory Activities by Compounds 6a−b, 6e−h, Sunitinib, and Erlotinib (2b)

compound	inhibition of $EGFR^{wt}$ kinase,[a] IC_{50} ± SD (nM)
6a	23 ± 4
6b	2.5 ± 0.3
6d	273 ± 35
6e	326 ± 46
6f	10 ± 3
6g	30 ± 5
6h	52 ± 6
sunitinib (**2e**)	140 ± 19
erlotinib (**2b**)	1.5 ± 2

[a]Values are expressed as the mean ± standard deviation (SD) from the dose−response curves of at least two independent experiments.

DOI: 10.1021/acs.jmedchem.8b01391
J. Med. Chem. XXXX, XXX, XXX−XXX

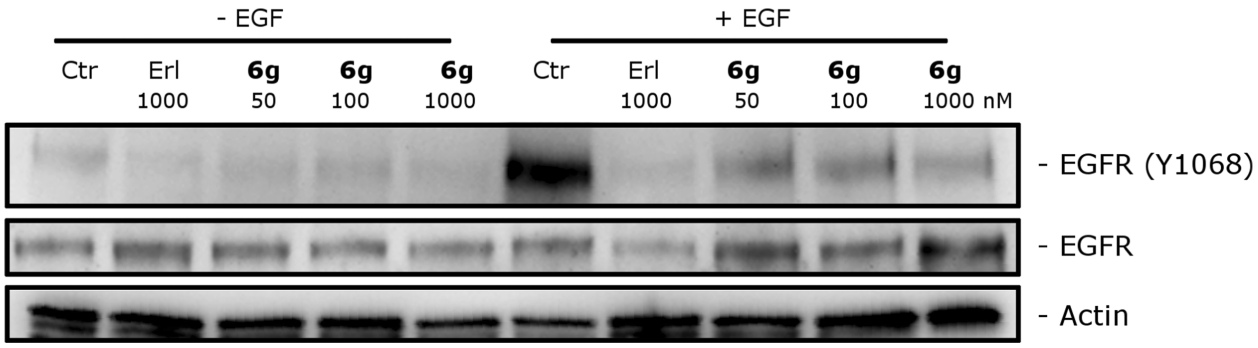

Figure 4. Effects of **6g** on EGFR signaling in HeLa cells. Cells were treated with the indicated concentrations of **6g** for 6 h and then stimulated by EGF (30 ng/mL) for 15 min. Cells were harvested for Western blot analysis for both EGFR and its phosphorylation at Y1068. Erlotinib (Erl) was used as the reference compound. We established that each gel lane had similar quantities of protein by determining their β-actin content.

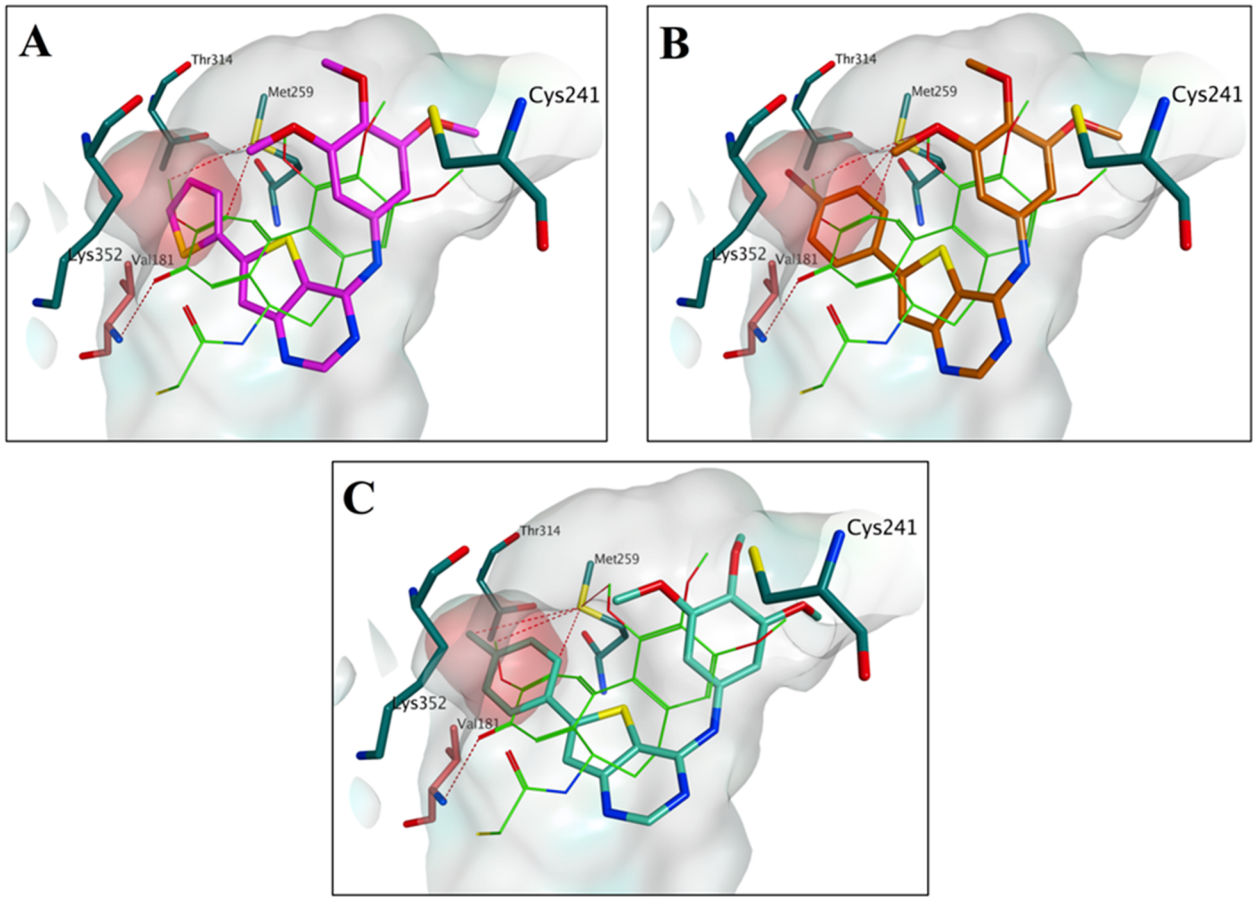

Figure 5. Proposed binding modes for compounds **6b** (A), **6e** (B), and **6g** (C) in comparison with DAMA-colchicine at the colchicine site (Protein Data Bank (PDB) ID: 1SA0). Carbons are shown in green for the cocrystallized DAMA-colchicine, in purple for compound **6b**, in orange for compound **6e**, and in turquoise for compound **6g**. The residues from the α-tubulin chain are shown in salmon, whereas residues from β-tubulin are colored in teal. The subpocket is highlighted with a red surface.

sunitinib as EGFR kinase inhibitors, with the 2-thienyl derivative **6b** as the most potent compound of the series. All evaluated molecules showed lower potency than erlotinib, with **6b** about 1.7-fold less potent. Three of these compounds (**6f–h**) were discovered to possess dual EGFR and tubulin polymerization inhibitory activity, and the good correlation between cytotoxicity and antitubulin activity extends to inhibition of EGFR activity.

Compound **6g**, with the most potent effect on tubulin polymerization, also exhibited excellent EGFR inhibitory activity, with IC_{50} values of 0.71 μM and 30 nM, respectively. In contrast, compound **6b**, the most active compound as an EGFR inhibitor (IC_{50}: 2.5 nM), was less potent as an inhibitor of tubulin polymerization (IC_{50}: 18 μM). As shown in Table 3, compounds **6d** and **6e** showed moderate EGFR inhibitory activities (IC_{50}: 273 and 326 nM, respectively) and similar potent antitubulin potency (IC_{50}: 3.3 and 2.5 μM), whereas for compound **6h**, a good correlation was observed between both its EGFR and antitubulin activities. The SAR analysis derived from the antiproliferative activities of compounds **6d** and **6e** was more consistent with their tubulin inhibition activities,

DOI: 10.1021/acs.jmedchem.8b01391
J. Med. Chem. XXXX, XXX, XXX−XXX

probably due to their potent inhibitory activities against tubulin polymerization but moderate activities against EGFR.

Compound 6g Induced Inhibition of EGFR Activation in HeLa Cells. To test the inhibition of the phosphorylation of EGFR and the downstream signaling pathway, we evaluated by Western blot analysis the inhibition of EGFR phosphorylation by **6g** in HeLa cells. The cells were treated with different concentrations of **6g** (10−1000 nM) and then stimulated with the epidermal growth factor (EGF) (50 ng/mL) for 15 min. The results (Figure 4) showed that **6g** strongly inhibited the phosphorylation of EGFR in a concentration-dependent manner starting at 50 nM. Erlotinib (1 μM) was taken as a reference compound, and erlotinib showed similar inhibitory activity to that of compound **6g**. These results demonstrated that **6g**, in addition to its antimitotic activity (see below), is also a potent EGFR inhibitor.

Molecular Modeling. A series of docking simulations were conducted on the newly designed 4-(3′,4′,5′-trimethoxyanilino)-6-substituted thieno[3,2-*d*]pyrimidines to evaluate their potential interaction at the binding site for colchicine on tubulin.[34] The results showed that the compounds bind at the active site with considerable overlap with *N*-deacetyl-*N*-(2-mercaptoacetyl)-colchicine (DAMA-colchicine), which was the ligand in the crystal structure, and the binding mode is consistent with the one previously reported for a thieno[2,3-*b*]pyridine series,[35] with the trimethoxyphenyl group in proximity of βCys241. The thieno[3,2-*d*]pyrimidine core overlapped with the central part of DAMA-colchicine, with the substituted phenyl ring placed in a small hydrophobic subpocket, potentially interacting with the surrounding amino acids βThr314, βVal181, and especially βMet259. This small subpocket appears to be able to interact with phenyl rings bearing different substituents, but only the *para*-methyl derivative **6g** has the correct combination of size/electronic properties to stably occupy and properly fit that area of the binding site (Figure 5C), suggesting a better inhibition of tubulin assembly. Replacement with a larger methoxy group (**6h**) does not allow the efficient occupation of the subpocket, indicating a potential reduction of the inhibition of tubulin polymerization. A similar decrease in activity is seen when the methyl group is replaced by different electron-withdrawing atoms (**6d−f**), but in this case, the decrease in activity could be associated with the electronic properties of the substituent rather than its size because they can occupy the subpocket very similarly to **6g** (Figure 5C). Compounds in which the para substituent has been removed (**6a**) or the phenyl ring has been replaced with a smaller five-member thiophene ring do not entirely fill the subpocket, potentially causing the 10−18-fold activity reduction found for these derivatives (Figure 5A).

In an attempt to clarify the binding mode of the new derivatives in the EGFR kinase domain, docking of the new molecules was performed using the crystal structure of the EGFR kinase domain in complex with the inhibitor (*R*)-6-(4-((4-ethylpiperazin-1-yl)methyl)phenyl)-*N*-(1-phenylethyl)-7*H*-pyrrolo[2,3-*d*]pyrimidin-4-amine (AEE788).[36] The 6-phenyl-thieno[3,2-*d*]pyrimidine core of the molecules perfectly overlaps with the phenyl pyrrolo[2,3-*d*]pyrimidine core of the cocrystallized inhibitor, making the same interactions with Gln791, Met793, and Leu844 that seem to anchor the molecule to the binding site (Figure 6). The trimethoxyphenyl group is placed in the same area occupied by the methyl moiety of AEE788, in proximity of Asp855.

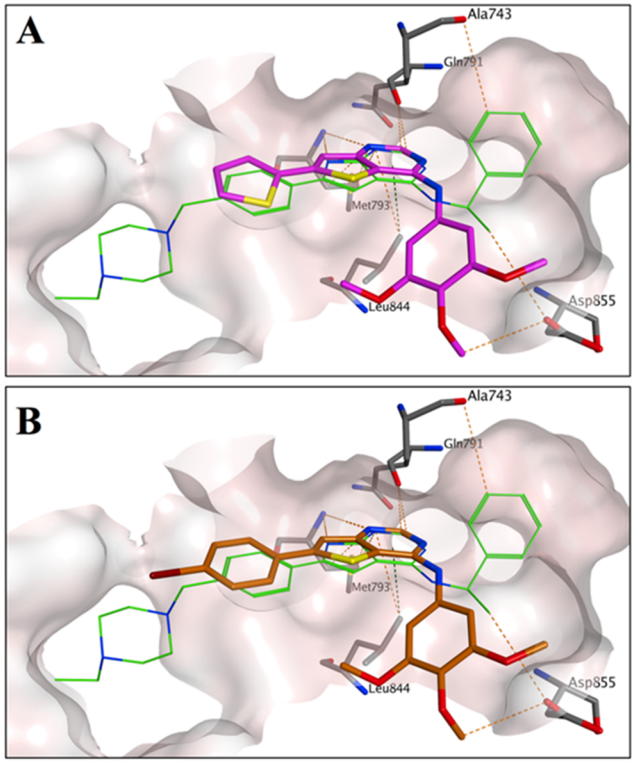

Figure 6. Proposed binding modes for compounds **6b** (A) and **6e** (B) in comparison with those for the inhibitor AEE788 in the crystal structure of the EGFR kinase domain (PDB ID: 2J6M). The carbons are shown in green for cocrystallized AEE788, in purple for compound **6b**, and in orange for compound **6e**. The phenyl ring of **6e** and the thiophene of **6b** are not involved in any interaction with the surrounding residues.

Overall, the binding mode proposed for these compounds is very similar to that of the cocrystallized ligand and also to that of another previously published thienopyrimidine EGFR inhibitor.[23] All of the new compounds occupy the active site in an identical manner. However, from these results, it is not possible to fully rationalize the role of the substitution on the phenyl ring in the anti-EGFR activity because that part of the molecule does not seem to be involved in any specific interactions with the binding pocket.

Effects of Compound 6g on the Cell Cycle. Cell cycle effects of the highly active **6g** were examined in HeLa and Jurkat cells, using flow cytometry (Figure 7). After 24 h, G2/M arrest occurred in both cell lines at 25 nM **6g**, as shown by propidium iodide (PI) staining. That the arrest occurred in mitosis was established by staining the cells with an immunofluorescent antibody to *p*-histone H3.[37] Typical histograms show that HeLa cells arrested in mitosis by **6g** are easily distinguished from G2 cells with the *p*-histone H3 stain (Figure 7D). The increase in mitotic cells (from 1.5% in the control) was especially dramatic with 50 (38%) and 100 (50%) nM **6g**.

Compound 6g Induced Apoptosis in Different Cell Lines. The mechanism of cell death was evaluated by two-dimensional cell sorting by staining DNA with PI and staining phosphatidylserine (PS) with a fluorescent annexin V derivative. We used two cell lines, Hela and Jurkat, in which we evaluated the effects of compound **6g** after both 24 and 48 h treatments. As shown in Figure 8, in both cell lines, **6g** caused apoptosis that increased with time and with **6g**

DOI: 10.1021/acs.jmedchem.8b01391
J. Med. Chem. XXXX, XXX, XXX−XXX

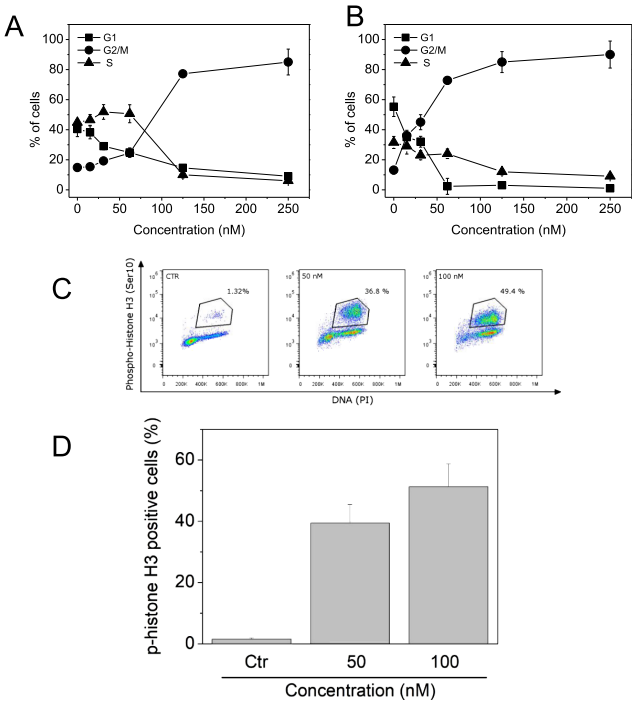

Figure 7. Cell cycle effects caused by **6g**: (A) HeLa cells treated with varying concentrations of **6g**, stained with PI, and examined by flow cytometry. (B) Jurkat cells treated with varying concentrations of **6g**, stained with PI, and examined by flow cytometry. G1 cells are indicated by the symbol ■, G2/M cells, by the symbol ●, and S cells, by the symbol ▲. Three independent experiments were performed, and the standard error of the mean (SEM) values are indicated. (C) Typical flow cytometric patterns of mitotic HeLa cells immunofluorescently stained with an antibody to *p*-histone H3, following treatment with 0 (left-hand pattern), 50 (middle pattern), or 100 (right-hand pattern) nM **6g**. (D) Histogram presentation of the data from (C) (two experiments, with SEM values indicated).

concentration, with an apoptotic effect observed at 50 nM, the lowest concentration used, shown in the 3-(4,5-dimethylthiazol-2-yl)-2,5-diphenyl tetrazolium bromide (MTT) test (Table 1).

Mitochondrial Depolarization and Formation of Reactive Oxygen Species Caused by Treatment with 6g. Mitochondria are critical for the occurrence of apoptosis.[38,39] Early in the process, the mitochondrial transmembrane potential ($\Delta\psi_{mt}$) changes. We measured these changes by flow cytometry through use of 5,5′,6,6′-tetrachloro-1,1′,3,3′-tetraethylbenzimidazolcarbocyanine (JC-1). As shown in Figure 9A, cells treated with different concentrations of **6g** (50, 100, and 250 nM) showed a concentration- and a time-dependent increase in the percentage of cells with low $\Delta\psi_{mt}$. The depolarization of the mitochondrial membrane is already evident at early times of drug exposure (3−6 h), in good agreement with findings of many microtubule-active agents that a fall in $\Delta\psi_{mt}$ occurs early in apoptosis in many types of cells.[40−42] We also established that this drop in $\Delta\psi_{mt}$ is associated with generation of reactive oxygen species (ROS)[43] (Figure 9B) following **6g** treatment for as short a time as 12 h with as little as 50 nM **6g**.

Compound 6g Induced Poly(ADP-ribose) Polymerase (PARP) Activation and Caused a Decrease in the Expression of Antiapoptotic Proteins. To gain a better insight into the mechanism of action of **6g**, we evaluated the cleavage of poly(ADP-ribose) polymerase (PARP) during the apoptotic process induced by this compound. As shown in Figure 10, compound **6g** in HeLa cells caused a concentration- and time-dependent cleavage of PARP, confirming its proapoptotic activity. Moreover, the expression of two antiapoptotic proteins, Bcl-2 and Mcl-1, was also studied.[44,45] Immunoblot analysis, shown in Figure 10, demonstrated that the expression of the antiapoptotic protein Bcl-2 was decreased, starting after a 24 h treatment at both 50 and 100 nM. The decrease in the expression of Mcl-1 was even greater, both at the lowest concentration and after the 24 h treatment.

Antivascular Activity of 6g. Combined use of cytotoxic drugs with agents showing antiangiogenic or antivascular effects to increase treatment effects is a relatively recent therapeutic strategy.[4] Many antitubulin drugs, especially CA-4P, were found to have vascular-disrupting effects against tumor endothelial cells.[46−49] We therefore examined effects of **6g** on human umbilical vein endothelial cells (HUVECs) to evaluate potential effects on angiogenesis. We specifically studied HUVECs growing in Matrigel, a substance rich in proangiogenic compounds, for their ability to alter their shape to resemble capillaries. Preliminary experiments carried out on these cells, with the aim to evaluate the cytotoxicity of the test compound, indicated that **6g** had a GI_{50} of 56 nM after a 48 h treatment. Thus, to evaluate antivascular activity, we used a concentration of **6g** that did not induce cellular death.

We examined the effects of 10 nM (noncytotoxic concentration) and 100 nM (cytotoxic concentration) **6g** on HUVECs after a 1 h treatment (Figure 11A). Both concentrations of **6g** disrupted the network formation observed in the untreated HUVECs. Standard image analysis[45] was performed to obtain the parameters usually evaluated: (1) nodes (Figure 11B), (2) master junctions (Figure 11C), (3) segment length (Figure 11D), (4) total branching length (Figure 11E), (5) number of meshes (Figure 11F), and (6) mesh area (Figure 11G).

The results for segment length and mesh area showed statistically significant effects for the lowest concentration used, suggesting the high potential of the vascular-disrupting activity of **6g**.

6g Induced Tumor Growth Reduction in a Mouse Allograft Tumor Model. In in vivo studies, tumor-bearing animals were dosed with **6g** every other day (q.o.d.) intraperitoneally, beginning on day 9. Two different doses (3.0 and 7.5 mg/kg) were studied, and CA-4P (30 mg/kg) was used as a reference compound. The murine allograft model was B16 murine melanoma cells injected into the flanks of mice.[50,51] The B16 melanoma cell line was used because it has high levels of EFGR kinase,[52,53] and, in initial experiments, we had found that the IC_{50} of **6g** was 23.4 ± 3.8 nM (MTT assay).

Figure 12A demonstrates that after four doses of **6g**, given on days 9, 11, 13, and 15, tumor burden was reduced 28% with 3.0 mg/kg and 52.5% with 7.5 mg/kg, as compared with a 34.9% reduction with 30 mg/kg CA-4P. No toxicity, based on no weight loss, was observed in any of the experimental groups (Figure 12B).

■ CONCLUSIONS

An effective strategy to develop anticancer agents is the discovery of synergistic multitargeting properties of new molecules. The thiophene ring has been employed as an isostere for benzene-fused pyrimidines in the design of

DOI: 10.1021/acs.jmedchem.8b01391
J. Med. Chem. XXXX, XXX, XXX−XXX

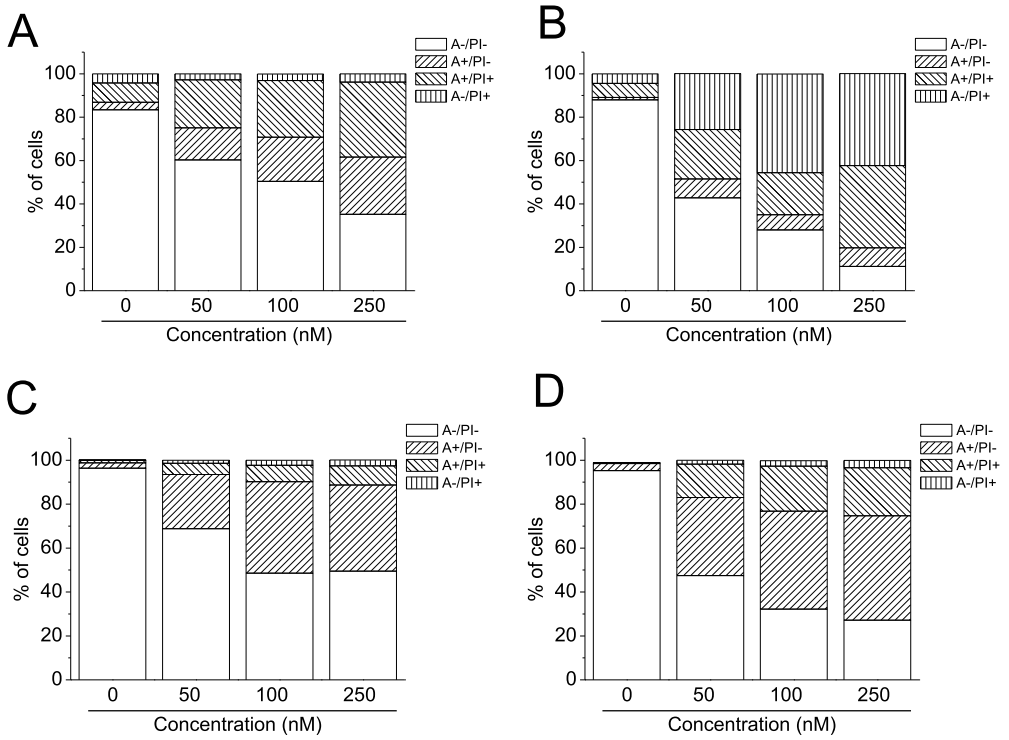

Figure 8. Apoptotic effects caused by **6g**: (A) Apoptosis examined by flow cytometry after treatment of HeLa cells for 24 h with **6g**, as indicated. (B) Apoptosis examined by flow cytometry after treatment of HeLa cells for 48 h with **6g**, as indicated. (C) Apoptosis examined by flow cytometry after treatment of Jurkat cells for 24 h with **6g**, as indicated. (D) Apoptosis examined by flow cytometry after treatment of Jurkat cells for 48 h with **6g**, as indicated. In all cases, cells were stained with annexin V linked to fluorescene and with PI.

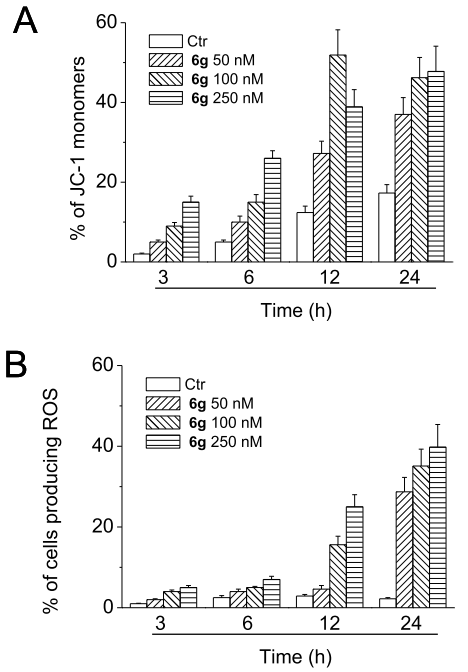

Figure 9. Flow cytometric measurement of $\Delta\psi_{mt}$ and ROS following treatment of HeLa cells with **6g**. Treatment times and **6g** concentrations are indicated: (A) Measurement of $\Delta\psi_{mt}$ by JC-1 fluorescence. (B) Measurement of ROS by fluorescence of 2,7-dichlorodihydrofluorescein diacetate.

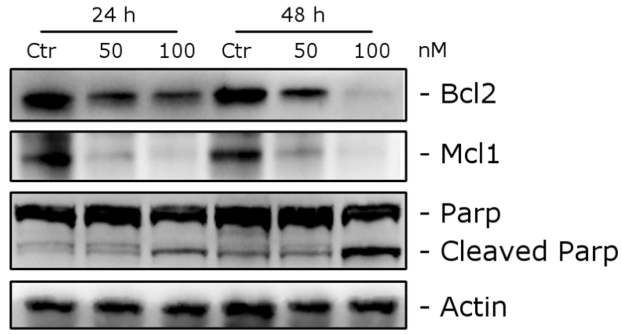

Figure 10. Western blot demonstrating PARP, Bcl-2, and Mcl-1 levels. HeLa cells were treated with **6g** as indicated. Equivalent protein loading was confirmed by evaluating anti-β-actin levels in the gel slots.

molecules that possess tyrosine kinase inhibitory activity. In this study, we report the design and synthesis of a new series of 4-(3′,4′,5′-trimethoxyanilino)-6-substituted thieno[3,2-*d*]-pyrimidines, some of which possess both tubulin polymerization and EGFR kinase inhibitory properties. The optimal structure at the phenyl ring at the C-6 position of the 4-(3′,4′,5′-trimethoxyanilino)-thieno[3,2-*d*]pyrimidine system was explored by various substituents, with either electron-releasing or electron-withdrawing properties. The importance of the specific substituent is demonstrated by the data summarized in Table 1.

Three of the 4-(3′,4′,5′-trimethoxyanilino)-6-substituted thieno[3,2-*d*]pyrimidine derivatives, corresponding to *p*-Cl (**6d**), *p*-Me (**6g**), and *p*-OMe (**6h**), were the most potent compounds found in this study, with IC_{50} values of, respectively, 3−600, 1−20, and 4−430 nM in the five cell lines. The 4-(3′,4′,5′-trimethoxyanilino)-6-(*p*-tolyl)thieno[3,2-*d*]pyrimidine derivative **6g** was the most potent compound of the whole series, exhibiting an IC_{50} value of 19 nM against the

DOI: 10.1021/acs.jmedchem.8b01391
J. Med. Chem. XXXX, XXX, XXX−XXX

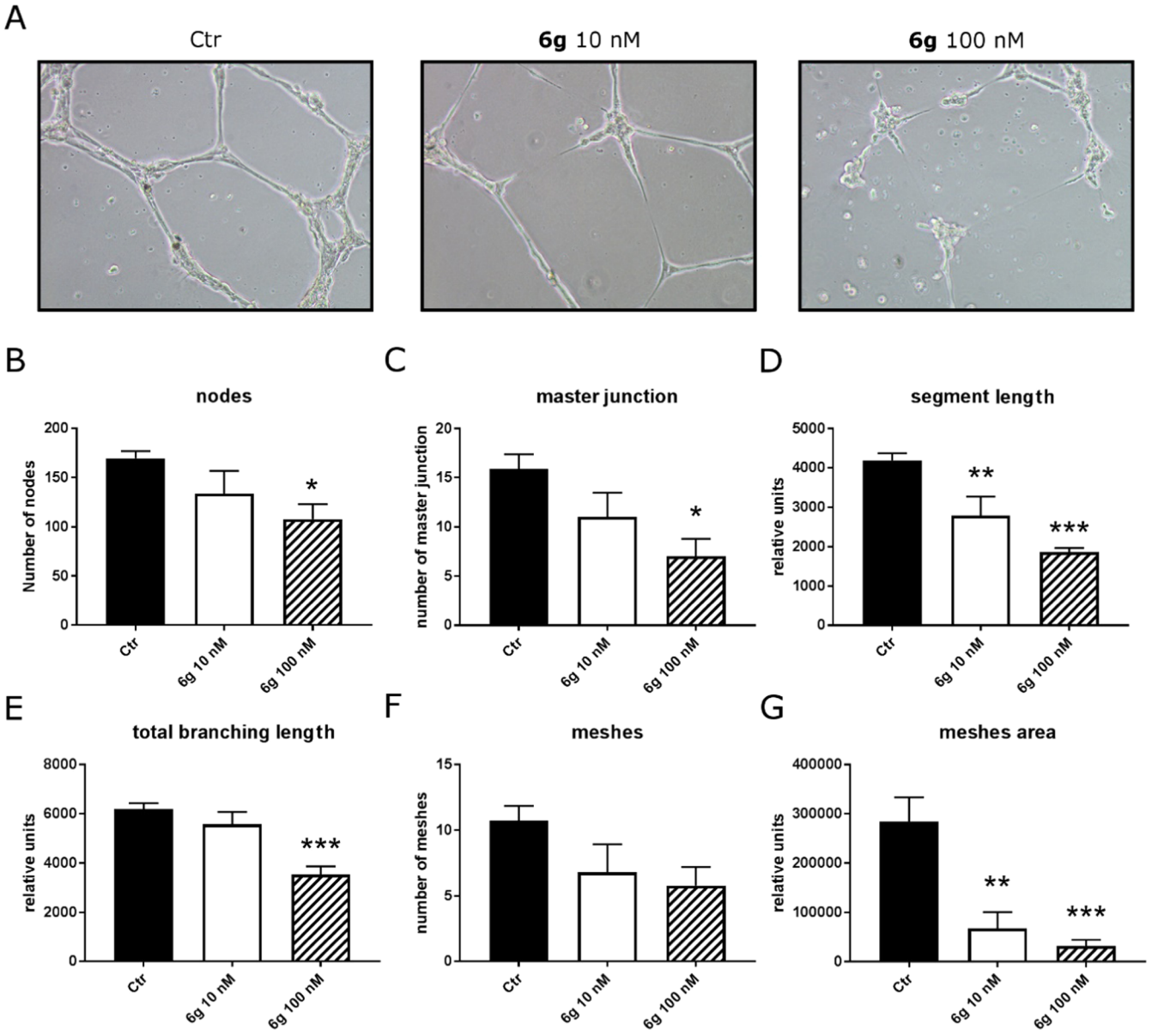

Figure 11. Antivascular effects of **6g** treatment on HUVECs. (A) Typical images after 1 h of growth on Matrigel of untreated cells (left-hand image), of cells treated with 10 nM **6g** (middle image), and of cells treated with 100 nM **6g** (right-hand image). (B–G) Quantitative evaluation of **6g** on standard parameters of HUVEC tubule formation, as indicated, at the indicated **6g** concentrations. Mean ± SEM, three experiments. ** $p < 0.01$; *** $p < 0.001$.

NSCLC A549 cell line, which harbors $EGFR^{wt}$ and K-ras mutations. Comparing the *p*-tolyl derivative **6g** with the *p*-methoxy phenyl compound **6h**, the latter was found to be 2–170-fold less active than **6g**, with the greatest differences in activity being 23- and 170-fold in A549 and Hela cells, respectively.

The corresponding thieno[2,3-*d*]pyrimidine isomers and the 2-anilino-7-(3′,4′,5′-trimethoxyanilino)thiazolo[4,5-*d*]-pyrimidine derivatives generally had little activity, with IC_{50} values usually greater than 10 μM. There was a considerable difference in potency between 4-(3′,4′,5′-trimethoxyanilino)-6-arylthieno[3,2-*d*]pyrimidine derivatives **6a**, **6d** (*p*-Cl), **6g** (*p*-Me), and **6h** (*p*-OMe) and the regioisomeric 4-(3′,4′,5′-trimethoxyanilino)-6-arylthieno[2,3-*d*]pyrimidine analogues **8d**, **8f**, **8i**, and **8k**, respectively, with these latter being considerably less active than the former in all cancer cell lines examined.

The inhibitory activity against EGFR and VEGFR-2 kinases of selected compounds **6a–b** and **6d–h** showed that these molecules were selective EGFR inhibitors. Compounds **6f–h** inhibited both EGFR kinase and tubulin polymerization, whereas derivative **6b** only inhibited EGFR kinase. Compounds **6a–b** and **6d–h** showed lower potency than erlotinib, with derivative **6b** having the greatest inhibitory activity against EGFR kinase, being only slightly less potent than erlotinib (IC_{50}: 2.5 and 1.5 nM, respectively). Besides its potent antiproliferative activity and high competitive inhibitory activity on EGFR, compound **6g** also inhibited tubulin assembly through an interaction at the colchicine site, thereby combining EGFR inhibition with antitubulin activity. The IC_{50} of 0.7 μM obtained with **6g** in the tubulin assembly assay was almost half of that obtained in simultaneous experiments with CA-4 (IC_{50}: 1.2 μM).

DOI: 10.1021/acs.jmedchem.8b01391
J. Med. Chem. XXXX, XXX, XXX–XXX

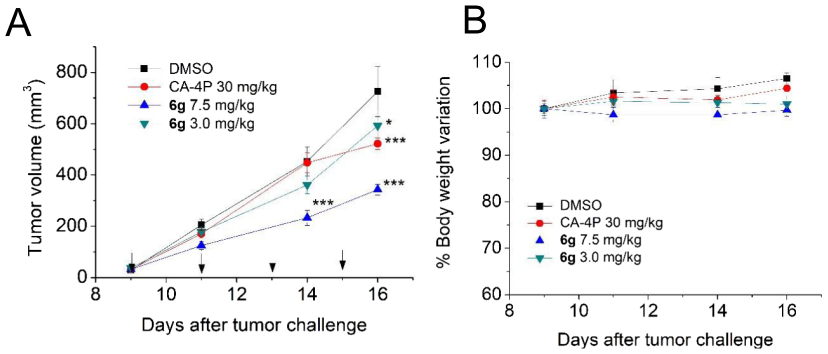

Figure 12. In vivo activity of **6g** in the treatment of murine B16 melanoma in an allograft model. (A) Each male C57BL/6 mouse was injected subcutaneously (s.c.) in its dorsum with 2.5 × 10^5 murine melanoma cells. On the days indicated by the arrows, mice were administered intraperitoneally (i.p.) with either vehicle 3.0 mg/kg **6g**, 7.5 mg/kg **6g**, or 30 mg/kg CA-4P. (B) Body weight variation after treatment with compound **6g** or CA-4P as described above. The data are plotted as mean ± SEM of tumor volume at each time point for five animals per group, * $p < 0.05$; *** $p < 0.001$ vs control.

In our results with compounds **6f–h**, there was a high correlation between the in vitro antiproliferative activity against the cancer cell lines and inhibition of tubulin polymerization and EGFR kinase, which suggested that targeting both tubulin and EGFR kinase played major roles in the cancer cell growth inhibitory effects of these three molecules.

EXPERIMENTAL SECTION

Chemistry. *General Materials and Methods.* A Varian VXR 200 spectrometer was used to obtain ^{1}H NMR data; a Varian Mercury Plus 400 spectrometer was used to obtain ^{13}C NMR data. Peak positions are provided in ppm (δ) downfield and J values in hertz. Mass spectra were obtained on a Waters ZQ 2000 electrospray ionization (ESI) single quadrupole mass spectrometer, with values given as $[M + 1]^+$. Melting points (mp) (uncorrected) were obtained on a Buchi–Tottoli instrument. Purity (≥95%) was verified by combustion elemental analyses performed at the Microanalytical Laboratory of the Department of Chemistry and Pharmaceutical Sciences of the University of Ferrara using a Yanagimoto MT-5 CHN recorder elemental analyzer. Thin-layer chromatography was performed on glass plates from Merck coated with silica gel 60 F_{254}, with compounds visualized by UV detection or with aqueous $KMnO_4$. Flash column chromatography was performed with 230–400-mesh silica gel and solvents as indicated. Organic solutions were dried over anhydrous Na_2SO_4. Commercial solvents and reagents were from Aldrich (Sigma-Aldrich) or Alfa Aesar (Johnson Matthey Company) and were used as supplied. Compounds **12a** and **12b** are commercially available. General procedures and references related to the preparation of methyl 3-aminothiophene-5-aryl/heteroaryl-2-carboxylate **9a–j**, ethyl 5-amino-2-anilinothiazole-4-carboxylate **9k–n**, and ethyl 2-aminothiophene-3-carboxylate **12c–l** derivatives are reported in the Supporting Information section. Active compounds were not recognized as pan-assay interference compounds according to the free ADME-tox filtering tool (FAF-Drugs4) program (http://fafdrugs4.mti.univ-paris-diderot.fr/).

General Procedure for the Synthesis of Compounds 6a–j, 7a–d, and 8a–l . A mixture of the appropriate 4-chlorothieno[3,2-*d*]pyrimidine **11a–j**, 7-chlorothiazolo[4,5-*d*]pyrimidine **11k–n**, or 4-chlorothieno[2,3-*d*]pyrimidine **14a–l** (1 mmol) and 3,4,5-trimethoxyaniline (2 mmol, 366 mg, 2 equiv) in isopropanol (5 mL) with a drop of concentrated HCl was refluxed for 18 h and then evaporated to dryness in vacuo. The residue was dissolved with dichloromethane, the organic solution was washed with water followed by brine and dried over Na_2SO_4, and the solvent was evaporated. The crude residue was purified by column chromatography on silica gel to furnish the desired compound.

6-Phenyl-N-(3,4,5-trimethoxyphenyl)thieno[3,2-d]pyrimidin-4-amine (6a). The crude residue was purified by flash chromatography, using ethyl acetate as eluent, to furnish **6a** as a yellow solid. Yield: 80%, mp 176 °C. ^{1}H NMR (dimethyl sulfoxide (DMSO)-d_6) δ: 3.67 (s, 3H), 3.79 (s, 6H), 7.22 (s, 2H), 7.51 (m, 3H), 7.85 (m, 2H), 7.90 (s, 1H), 8.59 (s, 1H), 9.64 (s, 1H). ^{13}C NMR (DMSO-d_6) δ: 55.84 (2C), 60.16, 100.17 (2C), 114.74, 120.50, 126.26 (2C), 129.42 (2C), 129.73, 132.62, 133.91, 135.03, 149.41, 152.57 (2C), 154.46, 154.81, 161.03. Mass spectrometry (MS) (ESI): $[M + 1]^+$ = 394.5. Anal. ($C_{21}H_{19}N_3O_3S$) C, H, N.

6-(Thiophen-2-yl)-N-(3,4,5-trimethoxyphenyl)thieno[3,2-d]-pyrimidin-4-amine (6b). The crude residue was purified by flash chromatography, using ethyl acetate/petroleum ether 9:1 (v/v) as eluent, to furnish **6b** as a yellow solid. Yield: 69%, mp 211 °C. ^{1}H NMR ($CDCl_3$) δ: 3.67 (s, 3H), 3.79 (s, 6H), 7.21 (s, 2H), 7.62 (dd, J = 5.0 and 1.2 Hz, 1H), 7.76 (m, 1H), 7.78 (s, 1H), 8.06 (dd, J = 5.0 and 1.2 Hz, 1H), 8.57 (s, 1H), 9.59 (s, 1H). ^{13}C NMR ($CDCl_3$) δ: 55.73 (2C), 60.06, 99.97 (2C), 113.98, 120.09, 123.76, 126.04, 128.28, 133.74, 134.07, 135.00, 144.26, 152.47 (2C), 154.36, 154.67, 160.94. MS (ESI): $[M + 1]^+$ = 400.5. Anal. ($C_{19}H_{17}N_3O_3S_2$) C, H, N.

6-(4-Fluorophenyl)-N-(3,4,5-trimethoxyphenyl)thieno[3,2-d]-pyrimidin-4-amine (6c). The crude residue was purified by flash chromatography, using ethyl acetate as eluent, to furnish **6c** as a brown solid. Yield: 68%, mp 192 °C. ^{1}H NMR (DMSO-d_6) δ: 3.65 (s, 3H), 3.77 (s, 6H), 7.19 (s, 2H), 7.37 (t, J = 9.2 Hz, 2H), 7.86 (s, 1H), 7.88 (m, 2H), 8.57 (s, 1H), 9.63 (bs, 1H). ^{13}C NMR (DMSO-d_6) δ: 56.30 (2C), 60.62, 10.67 (2C), 115.18, 116.81, 117.03, 121.13, 128.95, 129.04, 129.75, 134.38, 135.44, 148.68, 153.02, 154.97, 155.26, 161.54, 162.07, 164.53. MS (ESI): $[M + 1]^+$ = 412.4. Anal. ($C_{21}H_{18}FN_3O_3S$) C, H, N.

6-(4-Chlorophenyl)-N-(3,4,5-trimethoxyphenyl)thieno[3,2-d]-pyrimidin-4-amine (6d). The crude residue was purified by flash chromatography, using ethyl acetate as eluent, to furnish **6d** as a white solid. Yield: 65%, mp 215 °C. ^{1}H NMR (DMSO-d_6) δ: 3.67 (s, 3H), 3.79 (s, 6H), 7.20 (s, 2H), 7.58 (d, J = 7.2 Hz, 2H), 7.86 (d, J = 7.2 Hz, 2H), 7.93 (s, 1H), 8.59 (s, 1H), 9.66 (s, 1H). ^{13}C NMR (DMSO-d_6) δ: 55.74 (2C), 60.06, 100.14 (2C), 114.80, 121.08 (2C), 127.86 (2C), 129.34 (2C), 131.43, 133.78, 134.18, 134.84, 147.80, 152.47, 154.44, 154.74, 160.87. MS (ESI): $[M + 1]^+$ = 428.9. Anal. ($C_{21}H_{18}ClN_3O_3S$) C, H, N.

6-(4-Bromophenyl)-N-(3,4,5-trimethoxyphenyl)thieno[3,2-d]-pyrimidin-4-amine (6e). The crude residue was purified by flash chromatography, using ethyl acetate as eluent, to furnish **6e** as a yellow solid. Yield: 68%, mp 219 °C. ^{1}H NMR (DMSO-d_6) δ: 3.67 (s, 3H), 3.79 (s, 6H), 7.20 (s, 2H), 7.71 (d, J = 7.8 Hz, 2H), 7.80 (d, J = 7.8 Hz, 2H), 7.95 (s, 1H), 8.59 (s, 1H), 9.66 (s, 1H). ^{13}C NMR (DMSO-d_6) δ: 55.75 (2C), 60.06, 100.14 (2C), 114.81, 121.08, 122.86, 128.09 (2C), 131.79, 132.25 (2C), 133.87, 134.86, 147.88, 152.47 (2C), 154.46, 154.75, 160.89. MS (ESI): $[M + 1]^+$ = 520.4. Anal. ($C_{21}H_{18}BrN_3O_3S$) C, H, N.

6-(4-Iodophenyl)-N-(3,4,5-trimethoxyphenyl)thieno[3,2-d]-pyrimidin-4-amine (6f). The crude residue was purified by flash

DOI: 10.1021/acs.jmedchem.8b01391
J. Med. Chem. XXXX, XXX, XXX–XXX

chromatography, using ethyl acetate/petroleum ether 8:2 (v/v) as eluent, to furnish **6f** as a yellow solid. Yield: 61%, mp 199 °C. ^{1}H NMR (DMSO-d_6) δ: 3.67 (s, 3H), 3.79 (s, 6H), 7.20 (s, 2H), 7.84 (d, J = 8.4 Hz, 2H), 7.88 (d, J = 8.4 Hz, 2H), 7.94 (s, 1H), 8.59 (s, 1H), 9.65 (s, 1H). ^{13}C NMR (DMSO-d_6) δ: 55.73 (2C), 60.05, 100.11 (2C), 114.72, 120.91 (2C), 126.14, 127.98 (2C), 129.33, 132.03, 133.84, 134.85, 138.07, 148.14, 152.46, 154.43, 154.72, 160.87. MS (ESI): $[M + 1]^+$ = 520.4. Anal. ($C_{21}H_{18}IN_3O_3S$) C, H, N.

6-(p-Tolyl)-N-(3,4,5-trimethoxyphenyl)thieno[3,2-d]pyrimidin-4-amine (6g). The crude residue was purified by flash chromatography, using ethyl acetate as eluent, to furnish **6g** as a yellow solid. Yield: 75%, mp 202 °C. ^{1}H NMR (DMSO-d_6) δ: 2.37 (s, 3H), 3.67 (s, 3H), 3.79 (s, 6H), 7.22 (s, 2H), 7.33 (d, J = 8.0 Hz, 2H), 7.74 (d, J = 8.0 Hz, 2H), 7.83 (s, 1H), 8.58 (s, 1H), 9.60 (s, 1H). ^{13}C NMR (DMSO-d_6) δ: 20.77, 55.73 (2C), 60.05, 99.99 (2C), 114.32, 119.63, 126.04 (2C), 129.78, 129.97 (2C), 133.75, 134.99, 139.47, 149.51, 152.46 (2C), 154.30, 154.64, 161.02. MS (ESI): $[M + 1]^+$ = 408.5. Anal. ($C_{22}H_{21}N_3O_3S$) C, H, N.

6-(4-Methoxyphenyl)-N-(3,4,5-trimethoxyphenyl)thieno[3,2-d]pyrimidin-4-amine (6h). The crude residue was purified by flash chromatography, using ethyl acetate as eluent, to furnish **6h** as a brown solid. Yield: 54%, mp 182 °C. ^{1}H NMR (DMSO-d_6) δ: 3.67 (s, 3H), 3.79 (s, 6H), 3.83 (s, 3H), 7.07 (d, J = 8.4 Hz, 2H), 7.21 (s, 2H), 7.76 (s, 1H), 7.83 (d, J = 8.8 Hz, 2H), 8.56 (s, 1H), 9.56 (s, 1H). ^{13}C NMR (DMSO-d_6) δ: 55.31, 55.75 (2C), 60.08, 99.97 (2C), 105.88, 109.63, 114.73 (2C), 118.87 (2C), 125.06, 127.64 (2C), 135.06, 149.46, 152.49, 154.30, 154.58, 160.39, 161.22. MS (ESI): $[M + 1]^+$ = 424.5. Anal. ($C_{22}H_{21}N_3O_4S$) C, H, N.

6-(3-Methoxyphenyl)-N-(3,4,5-trimethoxyphenyl)thieno[3,2-d]pyrimidin-4-amine (6i). The crude residue was purified by flash chromatography, using ethyl acetate as eluent, to furnish **6i** as a yellow solid. Yield: 62%, mp 163 °C. ^{1}H NMR (DMSO-d_6) δ: 3.67 (s, 3H), 3.78 (s, 6H), 3.86 (s, 3H), 7.08 (m, 1H), 7.14 (s, 2H), 7.43 (m, 3H), 7.94 (s, 1H), 8.59 (s, 1H), 9.63 (s, 1H). ^{13}C NMR (DMSO-d_6) δ: 55.35, 55.85 (2C), 60.16, 100.05 (2C), 111.47, 114.77, 115.56, 118.55, 120.85, 130.61, 133.86, 133.95, 135.08, 149.22, 152.57 (2C), 154.48, 154.78, 159.86, 160.95. MS (ESI): $[M + 1]^+$ = 424.5. Anal. ($C_{22}H_{21}N_3O_4S$) C, H, N.

6-(4-Nitrophenyl)-N-(3,4,5-trimethoxyphenyl)thieno[3,2-d]pyrimidin-4-amine (6j). The crude residue was purified by flash chromatography, using ethyl acetate as eluent, to furnish **6j** as a yellow solid. Yield: 79%, mp > 300 °C. ^{1}H NMR (DMSO-d_6) δ: 3.67 (s, 3H), 3.80 (s, 6H), 7.21 (s, 3H), 8.12 (d, J = 9.0 Hz, 2H), 8.17 (s, 1H), 8.35 (d, J = 9.0 Hz, 2H), 8.63 (s, 1H), 9.78 (s, 1H). ^{13}C NMR ($CDCl_3$) δ: 55.77 (2C), 60.06, 78.53, 78.86, 79.19, 100.32 (2C), 123.48, 124.54 (2C), 127.27 (2C), 134.67, 138.68, 147.53, 152.50 (2C), 154.68, 154.91, 160.63. MS (ESI): $[M + 1]^+$ = 439.4. Anal. ($C_{21}H_{18}N_4O_5S$) C, H, N.

General Procedure for the Preparation of Compounds 10a−n and 13a−l . A mixture of the appropriate methyl 3-aminothiophene-5-aryl/heteroaryl-2-carboxylate **9a−j**, ethyl 5-amino-2-anilinothiazole-4-carboxylate **9k−n** or ethyl 2-aminothiophene-3-carboxylate derivatives **12a−l** (10 mmol) and formamide (15 mL) was heated at 180 °C for 18 h. After cooling to room temperature, cooled water (15 mL) was added to the reaction mixture. The solid was removed by filtration, washed with water and dried under vacuum for 12 h. The crude residue was suspended in ethyl ether, stirred for 30 min and filtered. The solid was used for the next reaction without further purification.

6-Phenylthieno[3,2-d]pyrimidin-4(3H)-one (10a). Yellow solid, yield: 71%, mp 294 °C. ^{1}H NMR (DMSO-d_6) δ: 7.48 (m, 3H), 7.35 (m, 3H), 8.17 (s, 1H), 12.6 (bs, 1H). MS (ESI): $[M + 1]^+$ = 229.3.

6-(Thiophen-2-yl)thieno[3,2-d]pyrimidin-4(3H)-one (10b). Black solid, yield: 95%, mp 170 °C. ^{1}H NMR (DMSO-d_6) δ: 7.63 (dd, J = 2.6 and 1.6 Hz, 1H), 7.74 (dd, J = 2.6 and 1.6 Hz, 1H), 8.01 (s, 1H), 8.10 (m, 1H), 8.15 (s, 1H), 12.2 (bs, 1H). MS (ESI): $[M + 1]^+$ = 235.3.

6-(4-Fluorophenyl)thieno[3,2-d]pyrimidin-4(3H)-one (10c). Brown solid, yield: 81%, mp > 300 °C. ^{1}H NMR (DMSO-d_6) δ: 7.34 (d, J = 8.8 Hz, 2H), 7.83 (s, 1H), 7.93 (m, 2H), 8.17 (s, 1H), 12.6 (bs, 1H). MS (ESI): $[M + 1]^+$ = 247.3.

6-(4-Chlorophenyl)thieno[3,2-d]pyrimidin-4(3H)-one (10d). Brown solid, yield: 89%, mp > 300 °C. ^{1}H NMR (DMSO-d_6) δ: 7.54 (d, J = 8.8 Hz, 2H), 7.87 (m, 3H), 8.17 (s, 1H), 11.6 (bs, 1H). MS (ESI): $[M + 1]^+$ = 263.7.

6-(4-Bromophenyl)thieno[3,2-d]pyrimidin-4(3H)-one (10e). Yellow solid, yield: 78%, mp > 300 °C. ^{1}H NMR (DMSO-d_6) δ: 7.67 (d, J = 8.6 Hz, 2H), 7.80 (d, J = 8.6 Hz, 2H), 7.90 (s, 1H), 8.17 (s, 1H), 12.6 (bs, 1H). MS (ESI): $[M + 1]^+$ = 308.2.

6-(4-Iodophenyl)thieno[3,2-d]pyrimidin-4(3H)-one (10f). Yellow solid, yield: 95%, mp > 300 °C. ^{1}H NMR (DMSO-d_6) δ: 7.63 (d, J = 8.8 Hz, 2H), 7.87 (m, 3H), 8.17 (s, 1H), 11.4 (bs, 1H). MS (ESI): $[M + 1]^+$ = 279.7.

6-(4-Tolyl)thieno[3,2-d]pyrimidin-4(3H)-one (10g). Brown solid, yield: 83%, mp > 300 °C. ^{1}H NMR (DMSO-d_6) δ: 2.36 (s, 3H), 7.29 (d, J = 7.8 Hz, 2H), 7.73 (m, 3H), 8.15 (s, 1H), 12.5 (bs, 1H). MS (ESI): $[M + 1]^+$ = 243.3.

6-(4-Methoxyphenyl)thieno[3,2-d]pyrimidin-4(3H)-one (10h). Brown solid, yield: >95%, mp > 300 °C. ^{1}H NMR (DMSO-d_6) δ: 3.82 (s, 3H), 7.03 (d, J = 8.8 Hz, 2H), 7.71 (s, 1H), 7.78 (d, J = 8.8 Hz, 2H), 8.14 (s, 1H), 11.8 (bs, 1H). MS (ESI): $[M + 1]^+$ = 259.3.

6-(3-Methoxyphenyl)thieno[3,2-d]pyrimidin-4(3H)-one (10i). Brown solid, yield: >95%, mp 212 °C. ^{1}H NMR (DMSO-d_6) δ: 3.84 (s, 3H), 7.04 (m, 1H), 7.39 (m, 2H), 7.88 (s, 1H), 7.94 (d, J = 8.6 Hz, 1H), 8.17 (s, 1H), 12.0 (bs, 1H). MS (ESI): $[M + 1]^+$ = 259.3.

6-(4-Nitrophenyl)thieno[3,2-d]pyrimidin-4(3H)-one (10j). Brown solid, yield: >95% yield, mp > 300 °C. ^{1}H NMR (DMSO-d_6) δ: 7.18 (d, J = 8.8 Hz, 2H), 7.43 (d, J = 8.8 Hz, 2H), 7.94 (s, 1H), 10.5 (bs, 1H), 11.4 (bs, 1H). MS (ESI): $[M + 1]^+$ = 274.3.

General Procedure for the Preparation of Compounds 11a−n and 14a−l . A mixture of the appropriate thieno[3,2-*d*]pyrimidin-4(3*H*)-one **10a−j**, thiazolo[4,5-*d*]pyrimidin-7(6*H*)-one **10k−n**, or thieno[2,3-*d*]pyrimidin-4(3*H*)-one **13a−l** (5 mmol) and $POCl_3$ (30 mL) with two to three drops of dimethylformamide was refluxed for 6 h. The mixture was cooled, $POCl_3$ was removed under vacuum, the residue obtained was poured into a saturated solution of $NaHCO_3$, and the suspension was neutralized with solid $NaHCO_3$. The mixture was extracted with dichloromethane and the organic phase was washed with water followed by brine, dried over Na_2SO_4, and concentrated in vacuo. The crude product was stirred for 15 min with ethyl ether (15 mL), and the desired product was obtained after removal of the ether by filtration.

4-Chloro-6-phenylthieno[3,2-d]pyrimidine (11a). Brown solid, yield: 71%, mp 152 °C. ^{1}H NMR (DMSO-d_6) δ: 7.57 (m, 3H), 6.01 (m, 2H), 8.25 (s, 1H), 9.03 (s, 1H). MS (ESI): $[M + 1]^+$ = 247.7.

4-Chloro-6-(thiophen-2-yl)thieno[3,2-d]pyrimidine (11b). Orange solid, yield: 60%, mp 176 °C. ^{1}H NMR (DMSO-d_6) δ: 7.79 (m, 2H), 8.11 (s, 1H), 8.36 (dd, J = 2.6 and 1.6 Hz, 1H), 9.00 (s, 1H). MS (ESI): $[M + 1]^+$ = 252.7.

4-Chloro-6-(4-fluorophenyl)thieno[3,2-d]pyrimidine (11c). Brown solid, yield: 83%, mp > 300 °C. ^{1}H NMR ($CDCl_3$) δ: 7.37 (d, J = 8.8 Hz, 2H), 8.04 (m, 2H), 8.11 (s, 1H), 9.03 (s, 1H). MS (ESI): $[M + 1]^+$ = 265.7.

4-Chloro-6-(4-chlorophenyl)thieno[3,2-d]pyrimidine (11d). Yellow solid, yield: 68%, mp 188 °C. ^{1}H NMR ($CDCl_3$) δ: 7.47 (d, J = 8.8 Hz, 2H), 7.69 (m, 3H), 8.96 (s, 1H). MS (ESI): $[M + 1]^+$ = 282.2.

6-(4-Bromophenyl)-4-chlorothieno[3,2-d]pyrimidine (11e). Yellow solid, yield: 55%, mp 201 °C. ^{1}H NMR (DMSO-d_6) δ: 7.75 (d, J = 9.0 Hz, 2H), 7.93 (d, J = 9.0 Hz, 2H), 8.29 (s, 1H), 9.04 (s, 1H). MS (ESI): $[M + 1]^+$ = 326.6.

4-Chloro-6-(4-iodophenyl)thieno[3,2-d]pyrimidine (11f). Yellow solid, yield: 54%, mp > 300 °C. ^{1}H NMR ($CDCl_3$) δ: 7.81 (d, J = 8.4 Hz, 2H), 7.95 (d, J = 8.4 Hz, 2H), 8.29 (s, 1H), 9.04 (s, 1H). MS (ESI): $[M + 1]^+$ = 373.6.

4-Chloro-6-(p-tolyl)thieno[3,2-d]pyrimidine (11g). Brown solid, yield: 84%, mp > 300 °C. ^{1}H NMR (DMSO-d_6) δ: 2.39 (s, 3H), 7.36

DOI: 10.1021/acs.jmedchem.8b01391
J. Med. Chem. XXXX, XXX, XXX−XXX

(d, J = 7.8 Hz, 2H), 7.87 (d, J = 7.8 Hz, 2H), 8.18 (s, 1H), 9.01 (s, 1H). MS (ESI): $[M + 1]^+$ = 261.7.

4-Chloro-6-(4-methoxyphenyl)thieno[3,2-d]pyrimidine (11h). Yellow solid, yield: 72%, mp 181 °C. ^{1}H NMR ($CDCl_3$) δ: 3.89 (s, 3H), 7.04 (d, J = 8.8 Hz, 2H), 7.69 (s, 1H), 7.71 (d, J = 8.8 Hz, 2H), 8.93 (s, 1H). MS (ESI): $[M + 1]^+$ = 277.7.

4-Chloro-6-(3-methoxyphenyl)thieno[3,2-d]pyrimidine (11i). Brown solid, yield: 61%, mp 153 °C. ^{1}H NMR ($CDCl_3$) δ: 3.87 (s, 3H), 7.14 (m, 1H), 7.76 (m, 3H), 8.29 (s, 1H), 9.04 (s, 1H). MS (ESI): $[M + 1]^+$ = 277.7.

4-Chloro-6-(4-nitrophenyl)thieno[3,2-d]pyrimidine (11j). Orange solid, yield: >95%, mp > 300 °C. ^{1}H NMR (DMSO-d_6) δ: 8.32 (d, J = 8.8 Hz, 2H), 8.36 (d, J = 8.8 Hz, 2H), 8.51 (s, 1H), 9.10 (s, 1H). MS (ESI): $[M + 1]^+$ = 292.7.

Biology and Materials and Methods. *Cytotoxicity Assays.* The cell lines and culture media used were described previously, as were the cell culture methodologies.[35] The 10 mM compound stock solutions were prepared with DMSO, and the DMSO concentration in cytotoxicity and all cell-based assays was always ≤0.25%.

Tubulin Assays. Assessment of compound effects on tubulin polymerization was described in detail previously,[53a] as was measurement of the binding of [^{3}H]colchicine to tubulin.[53b] For the polymerization assay, 10 μM purified bovine brain tubulin was used, and the extent of assembly after a 20 min incubation at 30 °C was the parameter measured. The reaction components in the colchicine assay included 1.0 μM tubulin, 5.0 μM [^{3}H]colchicine, and 1.0 or 5.0 μM potential inhibitors.

EGFR and VEGFR Kinase Activity Assays. Kinase assays were performed using the bioluminescent ADP-Glo kinase assay (Promega, Milano Italy), following the manufacturer's instructions. The assay was performed with the test compounds at different scalar concentrations. The IC_{50} values reported are based on the average of at least two titration curves. As reference compounds, erlotinib (Sigma-Aldrich) and sunitinib (Selleckchem) were used.

Molecular Modeling. Hardware, software, and general methodology were described in detail previously.[51,54,55] Protein structures were downloaded from the PDB (http://www.rcsb.org/; PDB codes 1SA0 and 2J6M, respectively, for tubulin and the EGFR kinase domain). The two proteins were preprocessed using the Schrödinger protein preparation wizard by assigning bond orders, adding hydrogens, and performing a restrained energy minimization of the added hydrogens using the OPLS_2005 force field. Ligand structures were built with molecular operating environment (MOE) and minimized using the MMFF94x force field. The ligands were then prepared using the Maestro LigPrep tool by energy minimizing the structures (OPLS_2005 force filed), generating possible ionization states at pH 7 ± 2 and generating tautomers and low-energy ring conformers. A 12 Å docking grid (inner box 10 Å and outer box 22 Å) was prepared using as centroid the cocrystallized DAMA-colchicine for the tubulin structure. A 15 Å docking grid (inner box 10 Å and outer box 25 Å) was prepared using as centroid the cocrystallized AEE788 for the EGFR structure. Molecular docking was performed using Glide SP keeping the default parameters and setting 5 as the number of output poses per input ligand to include in the solution. The docking results were visually inspected on MOE for the ability of molecules to bind the active sites.

Cell Cycle Distribution Evaluated by Flow Cytometry. HeLa or Jurkat cells (50 000 cells) were exposed to compounds for 24 h. Cells were harvested by centrifugation and fixed with 70% (v/v) ethanol (0 °C). Cells were lysed with 0.1% (v/v) Triton X-100 containing RNase A and stained with PI. A Beckman Coulter Cytomics FC500 instrument and MultiCycle for Windows software from Phoenix Flow Systems were used to analyze the cells.

Measurement of Apoptosis by Flow Cytometry. In these studies, the Cytomics FC500 instrument was used. The cells were stained with both PI, to stain DNA, and annexin V-fluorescein isothiocyanate, to stain membrane PS on the cell surface (which occurs in apoptosis). The latter was done following the instructions of the manufacturer (Roche Diagnostics) of the Annexin-V-Fluos reagent.

Evaluation of Cellular Protein Expression with Western Blots. Following growth for various times in the presence of **6g**, HeLa cells were harvested by centrifugation and washed twice in 0 °C phosphate-buffered saline (PBS). In some experiments, Hela cells were treated with **6g** or erlotinib (Sigma-Aldrich) and stimulated with EGF (R&D Systems, Minneapolis, MN), 50 ng/mL, for 15 min and then processed as described above. Cells were lysed with 0.1% (v/v) Triton X-100 containing RNase A at 0 °C, and supernatants were obtained by centrifuging the lysed cells at 15 000g for 10 min at 4 °C. The protein content of the solutions was measured, and 10 μg of protein from each sample was subjected to sodium dodecyl sulfate-polyacrylamide gel electrophoresis. Proteins were transferred by electroblotting to a poly(vinylidene difluoride) Hybond-P membrane from GE Healthcare. The membranes were treated with 5% bovine serum albumin in PBS containing 0.1% Tween 20 overnight at 4 °C. The membranes were then exposed for 2 h at room temperature to primary antibodies directed against PARP, Mcl-1, Bcl-2 (all from Cell Signaling), or β-actin (Sigma-Aldrich; to verify equal protein loading) and subsequently for 1 h to peroxidase-labeled secondary antibodies. The membranes were visualized using ECL select (GE Healthcare), and images were acquired using an Uvitec-Alliance imaging system.

Use of HUVECs as a Model for Antivascular Activity. Adherent HUVECs were obtained and cultured as before.[46,49] Once confluent, the cells were removed from the culture matrix with a trypsin−ethylenediaminetetraacetic acid solution and used up to the sixth passage.

Matrigel matrix (Basement Membrane Matrix, BD Biosciences) was prepared and left for 3 h at 4 °C. At this point, 230 μL of the matrix preparation was added to each well of a 24-well plate. The matrix was allowed to gel at 37 °C for 30 min. The matrix in each well was overlaid with 500 μL of medium containing 6000 HUVECs, which was incubated for 6 h to allow the formation of capillary tubes. Different concentrations of **6g** were added, and the cultures were incubated for another hour to monitor the disappearance of existing vasculature. The cultures were photographed (the four quadrants and the center of each well) at 10× magnification (phase contrast). The images were saved as TIFF files and anfalyzed with ImageJ image analysis software. Standard dimensional parameters (percent area covered by HUVECs and total length of the HUVEC network per field) were noted, and standard topological parameters (number of meshes and branching points per field) were estimated.[46,49]

In Vivo Activity of 6g . Animal procedures and care were performed in accord with institutional guidelines complying with all national and international laws and policies (EEC Council Directive 86/609, OJ L 358, December 12, 1987) and with "ARRIVE" guidelines (Animals in Research Reporting in Vivo Experiments). Six-week old C57BL/6 mice (from Charles River) were injected s.c. into the dorsolateral flank with 200 μL of PBS containing 25 000 BL6−B16 murine melanoma cells. Tumors became palpable on the 9th day, and animals were given q.o.d. × 4 i.p. injections of test compounds dissolved in 50 μL of DMSO at desired doses. Tumors were measured in two dimensions, and tumor volume was calculated using the formula $V = (D \times d^2)/2$, where D and d are the major and minor perpendicular tumor diameters.

■ ASSOCIATED CONTENT

Supporting Information

The Supporting Information is available free of charge on the ACS Publications website at DOI: 10.1021/acs.jmedchem.8b01391.

Antiproliferative activities of compounds **7a−d** (Table 1S) and **8a−l** (Table 2S); general procedures and references related to the preparation of methyl 3-aminothiophene-5-aryl/heteroaryl-2-carboxylate **9a−j**, ethyl 5-amino-2-anilinothiazole-4-carboxylate **9k−n**, and ethyl 2-aminothiophene-3-carboxylate **12c−l** derivatives; spectral data for the newly synthesized compounds **7a−d**, **10k−n**, **11k−n**, **13a−l**, and **14a−l**; ^{1}H

DOI: 10.1021/acs.jmedchem.8b01391
J. Med. Chem. XXXX, XXX, XXX−XXX

NMR and ^{13}C NMR spectra of compounds **6a−j**; elemental microanalyses for compounds **6a−j**, **7a−d**, and **8a−l** (PDF)

6b−e−g-docking-1SA0 (PDB)

6b−e-docking-2J6M (PDB)

Molecular formula strings (CSV)

AUTHOR INFORMATION

Corresponding Authors

*E-mail: rmr@unife.it. Phone: 39-(0)532-455303. Fax: 39-(0)532-455953 (R.R.).

*E-mail: lcarlotalopez@ugr.es. Phone: 34-(0)958-243849. Fax: 34-(0)958-243845 (L.C.L.-C.).

*E-mail: giampietro.viola1@unipd.it. Phone: 39-(0)49-8215485. Fax: 39-(0)49-8211462 (G.V.).

ORCID

Romeo Romagnoli: 0000-0002-6374-773X

Luisa Carlota Lopez-Cara: 0000-0003-1142-6448

Andrea Brancale: 0000-0002-9728-3419

Notes

The authors declare no competing financial interest.

The content of this paper is solely the responsibility of the authors and does not necessarily reflect the official views of the National Institutes of Health.

ACKNOWLEDGMENTS

We wish to thank Alberto Casolari for technical assistance. We also acknowledge the support of the Life Science Research Network Wales grant no. NRNPGSep14008, an initiative funded through the Welsh Government's Ser Cymru program, and "Proyecto de Excelencia de la Consejería de Innovación y Ciencia de la Junta de Andalucía, Spain ref P12-CTS-696," for its financial support.

ABBREVIATIONS

CA-4, combretastatin A-4; CA-4P, combretastain A-4 disodium phosphate; $\Delta\psi_{mt}$, mitochondrial transmembrane potential; DAMA-colchicine, *N*-deacetyl-*N*-(2-mercaptoacetyl)-colchicine; DMEM, Dulbecco's modified Eagle's medium; DMSO, dimethyl sulfoxide; EGF, epidermal growth factor; $EGFR^{wt}$, epidermal growth factor receptor wild type; ERG, electron-releasing group; ESI, electrospray ionization; EWG, electron-withdrawing group; HER, human epidermal growth factor receptor; JC-1, 5,5′,6,6′-tetrachloro-1,1′,3,3′-tetraethylbenzimidazolcarbocyanine; MTT, 3-(4,5-dimethylthiazol-2-yl)-2,5-diphenyl tetrazolium bromide; NSCLC, non-small-cell lung cancer; PARP, poly(ADP-ribose) polymerase; PBS, phosphate-buffered saline; PI, propidium iodide; ROS, reactive oxygen species; SAR, structure−activity relationship; HUVEC, human umbilical vein endothelial cell; VEGFR-2, vascular endothelial growth factor receptor-2

REFERENCES

(1) (a) Akhmanova, A.; Steinmetz, M. O. Control of microtubule organization and dynamics: two ends in the limelight. *Nat. Rev. Mol. Cell. Biol.* **2015**, *16*, 711−726. (b) Brouhard, G. J.; Rice, L. M. The contribution of $\alpha\beta$-tubulin curvature to microtubule dynamics. *J. Cell Biol.* **2014**, *207*, 323−334.

(2) (a) Vindya, N. G.; Sharma, N.; Yadav, M.; Ethiraj, K. R. Tubulins-the target for anticancer therapy. *Curr. Top. Med. Chem.* **2015**, *15*, 73−82. (b) Nitika, V.; Kapil, K. Microtubule targeting agents: a benchmark in cancer therapy. *Curr. Drug Ther.* **2014**, *8*, 189−196.

(3) (a) Patil, P. O.; Patil, A. G.; Rane, R. A.; Patil, P. C.; Deshmukh, P. K.; Bari, S. B.; Patil, D. A.; Naphade, S. S. Recent advancement in discovery and development of natural product combretastatin-inspired anticancer agents. *Anti-Cancer Agents Med. Chem.* **2015**, *15*, 955−969. (b) Mukhtar, E.; Adhami, V. M.; Mukhtar, H. Targeting microtubules by natural agents for cancer therapy. *Mol. Cancer Ther.* **2014**, *13*, 275−284.

(4) (a) Porcù, E.; Bortolozzi, R.; Basso, G.; Viola, G. Recent advances in vascular disrupting agents in cancer therapy. *Future Med. Chem.* **2014**, *6*, 1485−1498. (b) Mita, M. M.; Sargsyan, L.; Mita, A. C.; Spear, M. Vascular disrupting agents in oncology. *Expert Opin. Invest. Drugs* **2013**, *22*, 317−328.

(5) (a) Pettit, G. R.; Singh, S. B.; Hamel, E.; Lin, C. M.; Alberts, D. S.; Garcia-Kendall, D. Isolation and structure of the strong cell growth and tubulin inhibitor combretastatin A-4. *Experientia* **1989**, *45*, 209−211. (b) Pettit, G. R.; Cragg, G. M.; Herald, D. L.; Schmidt, J. M.; Lohavanijaya, P. Isolation and structure of combretastatin. *Can. J. Chem.* **1982**, *60*, 1374−1376.

(6) Lin, C. M.; Ho, H. H.; Pettit, G. R.; Hamel, E. Antimitotic natural products combretastatin A-4 and combretastatin A-2: studies on the mechanism of their inhibition of the binding of colchicine to tubulin. *Biochemistry* **1989**, *28*, 6984−6991.

(7) Liu, P.; Qin, Y.; Wu, L.; Yang, S.; Li, N.; Wang, H.; Xu, H.; Sun, K.; Zhang, S.; Han, X.; Sun, Y.; Shi, Y. A phase I clinical trial assessing the safety and tolerability of combretastatin A4 phosphate injections. *Anti-Cancer Drugs* **2014**, *25*, 462−471.

(8) (a) Patil, P. O.; Patil, A. G.; Rane, R. A.; Patil, P. C.; Deshmukh, P. K.; Bari, S. B.; Patil, D. A.; Naphade, S. S. Recent advancement in discovery and development of natural product combretastatin-inspired anticancer agents. *Anti-Cancer Agents Med. Chem.* **2015**, *15*, 955−969. (b) Rajak, H.; Dewangan, P. K.; Patel, V.; Jain, D. K.; Singh, A.; Veerasamy, R.; Sharma, P. C.; Dixit, A. design of combretastatin A-4 analogs as tubulin targeted vascular disrupting agent with special emphasis on their cis-restricted isomers. *Curr. Pharm. Des.* **2013**, *19*, 1923−1955.

(9) Greene, L. M.; Meegan, M. J.; Zisterer, D. M. Combretastatins: more than just vascular targeting agents? *J. Pharmacol. Exp. Ther.* **2015**, *355*, 212−227.

(10) Field, J. J.; Kanakkanthara, A.; Miller, J. H. Microtubule-targeting agents are clinically successful due to both mitotic and interphase impairment of microtubule function. *Bioorg. Med. Chem.* **2014**, *22*, 5050−5059.

(11) (a) Goffin, J. R.; Zbuk, K. Epidermal growth factor receptor: pathway, therapies, and pipeline. *Clin. Ther.* **2013**, *35*, 1282−1303. (b) Reardon, D. A.; Wen, P. Y.; Mellinghoff, I. K. Targeted molecular therapies against epidermal growth factor receptor: past experiences and challenges. *Neuro Oncol.* **2014**, *16*, viii7−viii13.

(12) Hynes, N. E.; Horsch, K.; Olayioye, M. A.; Badache, A. The ErbB receptor tyrosine family as signal integrators. *Endocr.-Relat. Cancer* **2001**, *8*, 151−159.

(13) (a) Hynes, N. E.; Lane, H. A. ERBB receptors and cancer: the complexity of targeted inhibitors. *Nat. Rev. Cancer* **2005**, *5*, 341−354. (b) Arteaga, C. L. Epidermal growth factor receptor dependence in human tumors: more than just expression? *Oncologist* **2002**, *7*, 31−39.

(14) Olayioye, M. A.; Neve, R. M.; Lane, H. A. N.; Hynes, N. E. The ErbB signaling network: receptor heterodimerization in development and cancer. *EMBO J.* **2000**, *19*, 3159−3167.

(15) (a) Zhang, H. Three generations of epidermal growth factor receptor tyrosine kinase inhibitors developed to revolutionize the therapy of lung cancer. *Drug Des., Dev. Ther.* **2016**, *10*, 3867−3872. (b) Hossam, M.; Lasheen, D. S.; Abouzid, K. A. Covalent EGFR inhibitors: binding mechanisms, synthetic approaches, and clinical profiles. *Arch. Pharm.* **2016**, *349*, 573−593. (c) Liu, F.; Tang, B.; Liu, H.; Li, L.; Liu, G.; Cheng, Y.; Xu, Y.; Chen, W.; Huang, Y. 4-Anilinoquinazoline derivatives with epidermal growth factor receptor inhibitor activity. *Anti-Cancer Agents Med. Chem.* **2016**, *16*, 1652−1664.

DOI: 10.1021/acs.jmedchem.8b01391
J. Med. Chem. XXXX, XXX, XXX−XXX

(16) (a) Herbst, R. S.; Heymach, J. V.; Lippman, S. M. Lung cancer. *N. Engl. J. Med.* **2008**, *359*, 1367−1380. (b) Di Maio, M.; Gridelli, C.; Normanno, N.; Perrone, F.; Ciardiello, F. Trying to compose the puzzle with all the pieces: epidermal growth factor tyrosine kinase inhibitors in non-small cell lung cancer. *J. Cell. Physiol.* **2005**, *205*, 355−363. (c) Cataldo, V. D.; Gibbons, D. L.; Perez-Soler, R.; Quintas-Cardama, A. Treatment of non-small-cell lung cancer with erlotinib or gefitinib. *N. Engl. J. Med.* **2011**, *364*, 947−955.

(17) (a) Yun, C. H.; Mengwasser, K. E.; Toms, A. V.; Woo, M. S.; Greulich, H.; Wong, K. K.; Meyerson, M.; Eck, M. J. The T790M mutation in EGFR kinase causes drug resistance by increasing the affinity for ATP. *Proc. Natl. Acad. Sci. U.S.A.* **2008**, *105*, 2070−2075. (b) Trusolino, L.; Bertotti, A. Compensatory pathways in oncogenic kinase signaling and resistance to targeted therapies: six degrees of separation. *Cancer Discovery* **2012**, *2*, 876−880.

(18) The identification numbers in https://clinicaltrials.gov websites are: NCT02326285, NCT00720304, NCT00049283, NCT02319577, NCT00083057, NCT01405079, NCT01755923, NCT00532441, NCT01749072, NCT01050322, NCT00446225, and NCT00553358 (accessed Oct 25, 2018).

(19) (a) Litvinov, V. P. The chemistry of thienopyrimidines. *Adv. Heterocycl. Chem.* **2006**, *92*, 83−143. (b) El-Ansary, A. K.; Kamal, A. M.; Al-Ghorafi, M. A. Synthesis and evaluation of 4-anilinoquinazoline bioisosteres as potential anti-breast cancer agents. *Eur. J. Med. Chem.* **2014**, *86*, 202−210. (c) Liu, Z.; Wu, S.; Wang, Y.; Li, R.; Wang, J.; Wang, L.; Zhao, Y.; Gong, P. Design, synthesis and biological evaluation of novel thieno[3,2-*d*]pyrimidine derivatives possessing diaryl semicarbazone scaffolds as potent antitumor agents. *Eur. J. Med. Chem.* **2014**, *87*, 782−799.

(20) (a) Bugge, S.; Kaspersen, S. J.; Larsen, S.; Nonstad, U.; Bjørkøy, G.; Sundby, E.; Hoff, B. H. Structure-activity study leading to identification of a highly active thienopyrimidine based EGFR inhibitor. *Eur. J. Med. Chem.* **2014**, *75*, 354−374. (b) Rheault, T. R.; Caferro, T. R.; Dickerson, S. H.; Donaldson, K. H.; Gaul, M. D.; Goetz, A. S.; Mullin, R. J.; McDonald, O. B.; Petrov, K. G.; Rusnak, D. W.; Shewchuk, L. M.; Spehar, G. H. M.; Truesdale, A. T.; Vanderwall, D. E.; Wood, E. R.; Uehling, D. E. Thienopyrimidine-based dual EGFR/ErbB-2 inhibitors. *Bioorg. Med. Chem. Lett.* **2009**, *19*, 817−820. (c) Beckers, T.; Sellmer, A.; Eichhorn, E.; Pongratz, H.; Schaechtele, C.; Totzke, F.; Kelter, G.; Krumbach, R.; Fiebig, H. H.; Boehmer, F. D.; Mahboobi, S. Novel inhibitors of epidermal growth factor receptor: (4-(arylamino)-7*H*-pyrrolo[2,3-*d*]pyrimidin-6-yl)-(1*H*-indol-2-yl)methanones and (1*H*-indol-2-yl)(4-(phenylamino) thieno[2,3-*d*]pyrimidin-6-yl)methanones. *Bioorg. Med. Chem.* **2012**, *20*, 125−136. (d) Milik, S. N.; Abdel-Aziz, A. K.; Lasheen, D. S.; Serya, R. A. T.; Minucci, S.; Abouzid, K. A. M. Surmounting the resistance against EGFR inhibitors through the development of thieno[2,3-*d*]pyrimidine-based dual EGFR/HER2 inhibitors. *Eur. J. Med. Chem.* **2018**, *155*, 316−336.

(21) Munchhof, M. J.; Beebe, J. S.; Casavant, J. M.; Cooper, B. A.; Doty, J. L.; Higdon, R. C.; Hillerman, S. M.; Soderstrom, C. I.; Knauth, E. A.; Marx, M. A.; Rossi, A. M.; Sobolov, S. B.; Sun, J. Design and SAR of thienopyrimidine and thienopyridine inhibitors of VEGFR-2 kinase activity. *Bioorg. Med. Chem. Lett.* **2004**, *14*, 21−24.

(22) Kemnitzer, W.; Sirisoma, N.; May, C.; Tseng, B.; Drewe, J.; Cai, S. X. Discovery of 4-anilino-*N*-methylthieno[3,2-*d*]pyrimidines and 4-anilino-*N*-methylthieno[2,3-*d*]pyrimidines as potent apoptosis inducers. *Bioorg. Med. Chem. Lett.* **2009**, *19*, 3536−3540.

(23) Bugge, S.; Buene, A. F.; Jurisch-Yaksi, N.; Moen, I. U.; Skjønsfjell, E. M.; Sundby, E.; Hoff, B. H. Extended structure-activity study of thienopyrimidine-based EGFR inhibitors with evaluation of drug-like properties. *Eur. J. Med. Chem.* **2016**, *107*, 255−274.

(24) Lin, R.; Johnson, S. G.; Connolly, P. J.; Wetter, S. K.; Binnun, E.; Hughes, T. V.; Murray, W. V.; Pandey, N. B.; Moreno-Mazza, S. J.; Adams, M.; Fuentes-Pesquera, A. R.; Middleton, S. A. Synthesis and evaluation of 2,7-diamino-thiazolo[4,5-*d*]pyrimidine analogues as anti-tumor epidermal growth factor receptor (EGFR) tyrosine kinase inhibitors. *Bioorg. Med. Chem. Lett.* **2009**, *19*, 2333−2337.

(25) (a) Cushman, M.; Nagarathnam, D.; Gopal, D.; He, H.-M.; Lin, C. M.; Hamel, E. Synthesis and evaluation of analogues of (*Z*)-1-(4-methoxyphenyl)-2-(3,4,5-trimethoxyphenyl)ethene as potential cytotoxic and antimitotic agents. *J. Med. Chem.* **1992**, *35*, 2293−2306. (b) Hatanaka, T.; Fujita, K.; Ohsumi, K.; Nakagawa, R.; Fukuda, Y.; Nihei, Y.; Suga, Y.; Akiyama, Y.; Tsuji, T. Novel B-ring modified combretastatin analogues: synthesis and antineoplastic activity. *Bioorg. Med. Chem. Lett.* **1998**, *8*, 3371−3374. (c) Negi, A. S.; Gautam, Y.; Alam, S.; Chanda, D.; Luqman, S.; Sarkar, J.; Khan, F.; Konwar, R. Natural antitubulin agents: Importance of 3,4,5-trimethoxyphenyl fragment. *Bioorg. Med. Chem.* **2015**, *23*, 373−389.

(26) Devambatla, R. K. V.; Choudhary, S.; Ihnat, M.; Hamel, E.; Mooberry, S. L.; Gangjee, A. Design, synthesis and preclinical evaluation of 5-methyl-N^4-aryl-furo[2,3-*d*]pyrimidines as single agents with combination chemotherapy potential. *Bioorg. Med. Chem. Lett.* **2018**, *28*, 3085−3093.

(27) Pavana, R. K.; Choudhary, S.; Bastian, A.; Ihnat, M. A.; Bai, R.; Hamel, E.; Gangjee, A. Discovery and preclinical evaluation of 7-benzyl-*N*-(substituted)-pyrrolo[3,2-*d*]pyrimidin-4-amines as single agents with microtubule targeting effects along with triple-acting angiokinase inhibition as antitumor agents. *Bioorg. Med. Chem.* **2017**, *25*, 545−556.

(28) Zhang, X.; Raghavan, S.; Ihnat, M.; Hamel, E.; Zammiello, C.; Bastian, A.; Mooberry, S. L.; Gangjee, A. The design, synthesis and biological evaluation of conformationally restricted 4-substituted-2,6-dimethylfuro[2,3-*d*]pyrimidines as multi-targeted receptor tyrosine kinase and microtubule inhibitors as potential antitumor agents. *Bioorg. Med. Chem.* **2015**, *23*, 2408−2423.

(29) Ihmaid, S.; Ahmed, H. E. A.; Zayed, M. F. The design and development of potent small molecules as anticancer agents targeting EGFR TK and tubulin polymerization. *Int. J. Mol. Sci.* **2018**, *19*, 408.

(30) Mphahlele, M. J.; Maluleka, M. M.; Parbhoo, N.; Malindisa, S. T. Synthesis, evaluation for cytotoxicity and molecular docking studies of benzo[*c*]furan-chalcones for potential to inhibit tubulin polymerization and/or EGFR-tyrosine kinase phosphorylation. *Int. J. Mol. Sci.* **2018**, *19*, 2552.

(31) Zayed, M. F.; Ahmed, S.; Ihmaid, S.; Ahmed, H. E. A.; Rateb, H. S.; Ibrahim, S. R. M. Design, synthesis, cytotoxic evaluation and molecular docking of new fluoroquinazolinones as potent anticancer agents with dual EGFR kinase and tubulin polymerization inhibitory effects. *Int. J. Mol. Sci.* **2018**, *19*, 1731.

(32) Zayed, M. F.; Rateb, H. S.; Ahmed, S.; Khaled, O. A.; Ibrahim, S. R. M. Quinazolinone-amino acid hybrids as dual inhibitors of EGFR kinase and tubulin polymerization. *Molecules* **2018**, *23*, 1699.

(33) Alswah, M.; Bayoumi, A. H.; Elgamal, K.; Elmorsy, A.; Ihmaid, S.; Ahmed, H. E. A. Design, synthesis and cytotoxic evaluation of novel chalcone derivatives bearing triazolo[4,3-*a*]-quinoxaline moieties as potent anticancer agents with dual EGFR kinase and tubulin polymerization inhibitory effects. *Molecules* **2018**, *23*, 48.

(34) Ravelli, R. B.; Gigant, B.; Curmi, P. A.; Jourdain, I.; Lachkar, S.; Sobel, A.; Knossow, M. Insight into tubulin regulation from a complex with colchicine and a stathmin-like domain. *Nature* **2004**, *428*, 198−202.

(35) Romagnoli, R.; Baraldi, P. G.; Kimatrai Salvador, M.; Preti, D.; Tabrizi, M. A.; Bassetto, M.; Brancale, A.; Hamel, E.; Castagliuolo, I.; Bortolozzi, R.; Basso, G.; Viola, G. Synthesis and biological evaluation of 2-alkoxycarbonyl-3-anilino benzo[*b*]thiophenes and thieno[2,3-*c*]pyridines as new potent anticancer agents. *J. Med. Chem.* **2013**, *56*, 2606−2618.

(36) Yun, C.-H.; Boggon, T. J.; Li, Y.; Woo, S.; Greulich, H.; Meyerson, M.; Eck, M. J. Structures of lung cancer-derived EGFR mutants and inhibitor complexes: mechanism of activation and insights into differential inhibitor sensitivity. *Cancer Cell* **2007**, *11*, 217−227.

(37) Goto, H.; Tomono, Y.; Ajiro, K.; Kosako, H.; Fujita, M.; Sakurai, M.; Okawa, K.; Iwamatsu, A.; Okigaki, T.; Takahashi, T.; Inagaki, M. Identification of a novel phosphorylation site on histone H3 coupled with mitotic chromosome condensation. *J. Biol. Chem.* **1999**, *274*, 25543−25549.

DOI: 10.1021/acs.jmedchem.8b01391
J. Med. Chem. XXXX, XXX, XXX−XXX

(38) Xiong, S.; Mu, T.; Wang, G.; Jiang, X. Mitochondria-mediated apoptosis in mammals. *Protein Cell* **2014**, *5*, 737−749.
(39) Rovini, A.; Savry, A.; Braguer, D.; Carré, M. Microtubule-targeted agents: when mitochondria become essential to chemotherapy. *Biochim. Biophys. Acta, Bioenerg.* **2011**, *1807*, 679−688.
(40) Mendez, G.; Policarpi, C.; Cenciarelli, C.; Tanzarella, C.; Antoccia, A. Role of Bim in apoptosis induced in H460 lung tumor cells by the spindle poison combretastatin-A4. *Apoptosis* **2011**, *16*, 940−949.
(41) Romagnoli, R.; Baraldi, P. G.; Kimatrai Salvador, M.; Preti, D.; Tabrizi, M. A.; Brancale, A.; Fu, X.-H.; Li, J.; Zhang, S.-Z.; Hamel, E.; Bortolozzi, R.; Porcù, E.; Basso, G.; Viola, G. Discovery and optimization of a series of 2-aryl-4-amino-5-(3′,4′,5′-trimethoxybenzoyl)thiazoles as novel anticancer agents. *J. Med. Chem.* **2012**, *55*, 5433−5445.
(42) Romagnoli, R.; Baraldi, P. G.; Kimatrai Salvador, M.; Prencipe, F.; Bertolasi, V.; Cancellieri, M.; Brancale, A.; Hamel, E.; Castagliuolo, I.; Consolaro, F.; Porcù, E.; Basso, G.; Viola, G. Synthesis, antimitotic and antivascular activity of 1-(3′,4′,5′-trimethoxybenzoyl)-3-arylamino-5-amino-1,2,4-triazoles. *J. Med. Chem.* **2014**, *57*, 6795−6808.
(43) Zamzami, N.; Marchetti, P.; Castedo, M.; Decaudin, D.; Macho, A.; Hirsch, T.; Susin, S. A.; Petit, P. X.; Mignotte, B.; Kroemer, G. Sequential reduction of mitochondrial transmembrane potential and generation of reactive oxygen species in early programmed cell death. *J. Exp. Med.* **1995**, *182*, 367−377.
(44) Wertz, I. E.; Kusam, S.; Lam, C.; Okamoto, T.; Sandoval, W.; Anderson, D. J.; Helgason, E.; Ernst, J. A.; Eby, M.; Liu, J.; Belmont, L. D.; Kaminker, J. S.; O'Rourke, K. M.; Pujara, K.; Kohli, P. B.; Johnson, A. R.; Chiu, M. L.; Lill, J. R.; Jackson, P. K.; Fairbrother, W. J.; Seshagiri, S.; Ludlam, M. J.; Leong, K. G.; Dueber, E. C.; Maecker, H.; Huang, D. C.; Dixit, V. M. Sensitivity to antitubulin chemotherapeutics is regulated by MCL1 and FBW7. *Nature* **2011**, *471*, 110−114.
(45) Czabotar, P. E.; Lessene, G.; Strasser, A.; Adams, J. M. Control of apoptosis by the BCL-2 protein family: implications for physiology and therapy. *Nat. Rev. Mol. Cell Biol.* **2014**, *15*, 49−63.
(46) Porcù, E.; Viola, G.; Bortolozzi, R.; Mitola, S.; Ronca, R.; Presta, M.; Persano, L.; Romagnoli, R.; Baraldi, P. G.; Basso, G. TR-644 a novel potent tubulin binding agent induces impairment of endothelial cells function and inhibits angiogenesis. *Angiogenesis* **2013**, *16*, 647−662.
(47) Romagnoli, R.; Baraldi, P. G.; Kimatrai Salvador, M.; Prencipe, F.; Bertolasi, V.; Cancellieri, M.; Brancale, A.; Hamel, E.; Castagliuolo, I.; Consolaro, F.; Porcù, E.; Basso, G.; Viola, G. Synthesis, antimitotic and antivascular activity of 1-(3′,4′,5′-trimethoxybenzoyl)-3-arylamino-5-amino-1,2,4-triazoles. *J. Med. Chem.* **2014**, *57*, 6795−6808.
(48) Romagnoli, R.; Baraldi, P. G.; Kimatrai Salvador, M.; Prencipe, F.; Lopez-Cara, C.; Schiaffino Ortega, S.; Brancale, A.; Hamel, E.; Castagliuolo, I.; Mitola, S.; Ronca, R.; Bortolozzi, R.; Porcù, E.; Basso, G.; Viola, G. Design, synthesis, in vitro and in vivo anticancer and antiangiogenic activity of novel 3-arylamino benzofuran derivatives targeting the colchicine site on tubulin. *J. Med. Chem.* **2015**, *58*, 3209−3222.
(49) Porcù, E.; Persano, L.; Ronca, R.; Mitola, S.; Bortolozzi, R.; Romagnoli, R.; Oliva, P.; Basso, G.; Viola, G. The novel antitubulin agent TR-764 strongly reduces tumor vasculature and inhibits HIF-1α activation. *Sci. Rep.* **2016**, *6*, No. 27886.
(50) Ronca, R.; Di Salle, E.; Giacomini, A.; Leali, D.; Alessi, P.; Coltrini, D.; Ravelli, C.; Matarazzo, S.; Ribatti, D.; Vermi, W.; Presta, M. Long pentraxin-3 inhibits epithelial-mesenchymal transition in melanoma cells. *Mol. Cancer Ther.* **2013**, *12*, 2760−2771.
(51) Romagnoli, R.; Baraldi, P. G.; Prencipe, F.; Oliva, P.; Oliva, P.; Oliva, P.; Oliva, P.; Ferla, S.; Brancale, A.; Hamel, E.; Ronca, R.; Bortolozzi, R.; Mariotto, E.; Basso, G.; Viola, G. Design and synthesis of potent in vitro and in vivo anticancer agents based on 1-(3′,4′,5′-trimethoxyphenyl)-2-aryl-1*H*-imidazole. *Sci. Rep.* **2016**, *6*, No. 26602.
(52) Xu, Q.; Zhang, X.; Yue, J.; Liu, C.; Cao, C.; Zhong, H.; Qingjun Ma, Q. Human TGFalpha-derived peptide TGFalphaL3 fused with superantigen for immunotherapy of EGFR-expressing tumours. *BMC Biotechnol.* **2010**, *10*, 91.
(53) (a) Hamel, E. Evaluation of antimitotic agents by quantitative comparisons of their effects on the polymerization of purified tubulin. *Cell Biochem. Biophys.* **2003**, *38*, 1−21. (b) Verdier-Pinard, P.; Lai, J.-Y.; Yoo, H.-D.; Yu, J.; Marquez, B.; Nagle, D. G.; Nambu, M.; White, J. D.; Falck, J. R.; Gerwick, W. H.; Day, B. W.; Hamel, E. Structure-activity analysis of the interaction of curacin A, the potent colchicine site antimitotic agent, with tubulin and effects of analogs on the growth of MCF-7 breast cancer cells. *Mol. Pharmacol.* **1998**, *53*, 62−67.
(54) *Molecular Operating Environment (MOE 2015.10)*; Chemical Computing Group, Inc.: Montreal, Quebec, Canada, 2015. http://www.chemcomp.com.
(55) *Schrödinger Release 2017-1: Maestro*; Schrödinger, LLC: New York, NY, 2017.

DOI: 10.1021/acs.jmedchem.8b01391
J. Med. Chem. XXXX, XXX, XXX−XXX